1-12-2024

Evaluation of First-Order Actuator Dynamics and Linear Controller for a Bio-Inspired Rotating Empennage Fighter Aircraft

Benjamin C. Moulton
Utah State University, ben.moulton@usu.edu

Matthew W. Harris
Utah State University, matthew.harris@usu.edu

Douglas F. Hunsaker
Utah State University, doug.hunsaker@usu.edu

James J. Joo
U.S. Air Force Research Laboratory

Recommended Citation

Moulton, B. C., Harris, M. W., Hunsaker, D. F., and Joo, J. J., "Evaluation of First-Order Actuator Dynamics and Linear Controller for a Bio-Inspired Rotating Empennage Fighter Aircraft," AIAA SciTech 2024 Forum, January 2024, AIAA-2024-2649 DOI: 10.2514/6.2024-2649

Evaluation of First-Order Actuator Dynamics and Linear Controller for a Bio-Inspired Rotating Empennage Fighter Aircraft

Benjamin C. Moulton*, Matthew W. Harris†, Douglas F. Hunsaker‡,
Utah State University, Logan, UT, 84321

and James J. Joo§
U.S. Air Force Research Laboratory, Wright-Patterson Air Force Base, Ohio, 45433-7402

This paper considers the problem of stabilizing a bio-inspired fighter aircraft variant at its Air Combat Maneuver Condition. The aircraft equations of motion are linearized, and an infinite-horizon linear quadratic regulator design is conducted for this aircraft. Included in the dynamics are first-order actuator models, which have the effect of slowing actuator responses. This is particularly important for the bio-inspired variant because it requires rotation of the empennage, which has relatively large inertia. The bio-inspired variant open-loop system is unstable in the short period and Dutch roll modes, which is mitigated in the closed-loop system. Monte Carlo simulation responses to initial condition dispersions, aerodynamic model errors, and atmospheric turbulence are presented for the controlled aircraft system. These simulations demonstrate the robust properties of the presented control design. Discussion is dedicated to control designs neglecting input from throttle and the rotating tail, and corresponding successes. Whereas the bio-inspired variant aircraft can be successfully controlled without rotating tail input, effects from neglecting throttle input show throttle should be included, but perhaps in an alternate loop such as a speed controller.

I. Introduction

NEXT-GENERATION aircraft will use novel structural, control, aerodynamic, and avionic techniques. One such proposed innovative design is the bio-inspired rotating empennage (BIRE), in which the vertical tail is removed from a statically-unstable baseline fighter aircraft similar to the F-16, and the empennage is allowed to rotate about the fuselage axis. This design has various advantages and limitations, reported in previous and contemporary work on attainable aerodynamic moments [1], structural design [2], static and dynamic stability [3, 4], static trim [5], and preliminary control analyses [6].

The governing dynamics for aircraft flight-simulation are called the equations of motion (EOM). These equations define the change over time of body-fixed velocities, body-fixed rotation rates, Earth-fixed position, and Earth-fixed orientation. Each of these parameters have an x-, y-, or z-related component, resulting in 12 states for the second order 6 degree-of-freedom (DOF) aircraft. As the EOM do not incorporate actuator dynamics, this analysis will incorporate additional equations describing the time rate-of-change of the first-order actuator response. Each actuator corresponds to one of the four control effectors on each aircraft: ailerons, stabilators, rudder / BIRE mechanism, and throttle setting. With feedback to these actuators the system can be controlled using optimal [7–11], nonlinear [12, 13], adaptive [14, 15], or other control methodologies.

The basic control methodology used in the present work is the infinite horizon linear quadratic regulator (LQR) method [16, 17]. This method entails minimizing quadratic costs based on weightings of the state and input incorporated with linear system dynamics in the algebraic Riccati equation. LQR controllers are often used in aircraft controller design [18–23], and have frequently been used to study the F-16 aircraft [24–33]. LQR techniques have also been used to study the effect of actuator dynamics on aircraft control design [22, 32–35]. Many have specifically studied the F-16 aircraft using actuator dynamics [36], additionally using LQR techniques [33, 37], with the fully-coupled nonlinear

*PhD Student, Mechanical and Aerospace Engineering, 4130 Old Main Hill, AIAA Student Member
†Assistant Professor, Mechanical and Aerospace Engineering, 4130 Old Main Hill, AIAA Senior Member
‡Associate Professor, Mechanical and Aerospace Engineering, 4130 Old Main Hill, AIAA Senior Member
§Senior Research Mechanical Engineer, AFRL/RQVS, 2790 D St., AIAA Senior Member

EOM [38]. This work will differ from these works through inspection of the control implications of removing the vertical tail from a statically unstable fighter aircraft and allowing the horizontal tail to rotate about the fuselage axis. A drawing of the BIRE is shown in Fig. 1.

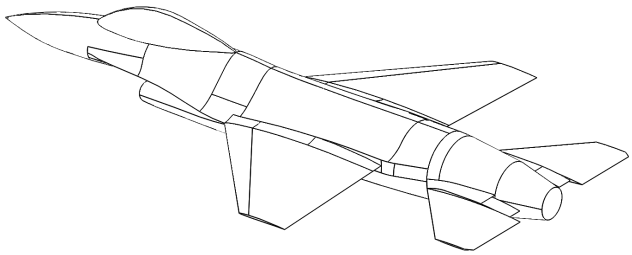

Fig. 1 Computer aided design drawing of the BIRE aircraft.

The simulation dynamics in the present work will use the aerodynamic models for the baseline and BIRE aircraft established by Bolander et al. [5] which were developed using low-order aerodynamic tools on the aircraft geometry reported by Nguyen et al. [39]. Previous control development in this body of work has focused on the development of a linearized system and preliminary controllability and analyses of simulation response to gusts [6]. The purpose of the present paper is to expand on previous control work, focusing on acceptable actuator design considering first-order actuator dynamics and actuation-limiting rates. In this manuscript the aircraft dynamics and actuation limits are studied through simulation using initial condition dispersions, aerodynamic model error, and atmospheric turbulence. The controller performance is also examined in frequency domain analyses.

II. Aircraft Dynamics Model Overview

The aircraft dynamics models for the baseline and BIRE aircraft depend on the aircraft states: velocity in body-fixed coordinates (axial velocity V_{x_b}, side velocity V_{y_b}, and normal velocity V_{z_b}), rotation rates in body-fixed coordinates (roll rate p, pitch rate q, and yaw rate r), position in Earth-fixed coordinates (x_f, y_f, z_f), and orientation in Earth-fixed coordinates (bank angle ϕ, elevation angle θ, and heading angle ψ). These states are aggregated in the state vector

$$x = \begin{bmatrix} V_{x_b} & V_{y_b} & V_{z_b} & p & q & r & x_f & y_f & z_f & \phi & \theta & \psi \end{bmatrix}^T \tag{1}$$

These models also depend on the aircraft control effectors, each of which have an actuator and commanded control component. The control effectors are: ailerons (δ_a), stabilators (δ_e for baseline / δ_e^B for BIRE), rudder / BIRE mechanism (δ_r / δ_B), and throttle setting (τ). These components are aggregated in the actuator state and control input vectors for the baseline aircraft as

$$\delta = \begin{bmatrix} \delta_a \\ \delta_e \\ \delta_r \\ \tau \end{bmatrix}, \quad u = \begin{bmatrix} \delta_{a\,cmd} \\ \delta_{e\,cmd} \\ \delta_{r\,cmd} \\ \tau_{cmd} \end{bmatrix} \tag{2}$$

and for the BIRE aircraft as

$$\delta = \begin{bmatrix} \delta_a \\ \delta_e^B \\ \delta_B \\ \tau \end{bmatrix}, \quad u = \begin{bmatrix} \delta_{a\,cmd} \\ \delta_{e\,cmd}^B \\ \delta_{B\,cmd} \\ \tau_{cmd} \end{bmatrix} \tag{3}$$

These equations also depend on the aerodynamic angles and total velocity

$$\alpha = \tan^{-1}\left(\frac{V_{z_b}}{V_{x_b}}\right) \tag{4}$$

$$\beta = \sin^{-1}\left(\frac{V_{y_b}}{V}\right) \tag{5}$$

$$V = \sqrt{V_{x_b}^2 + V_{y_b}^2 + V_{z_b}^2} \tag{6}$$

where α is the angle of attack, β is the side-slip angle, and V is the total freestream velocity. Compressibility is accounted for in the model via a correction factor, which is a function of mach number M. Mach number is the ratio of the total velocity V and the freestream speed of sound a:

$$M = \frac{V}{a} \tag{7}$$

Some terms on which the models depend and are referenced later are the freestream air density ρ, main wing area S_w, main-wing mean aerodynamic chord $\bar{c}_w$, and main wing span b_w. The freestream air density and speed of sound are determined using a standard atmosphere model [40].

These aircraft states, inputs, and aircraft and freestream properties will be the fundamental parameters of the aircraft model. The aircraft models will be described in the order in which equations are applied. First, the incompressible aerodynamics of each aircraft are determined from the aircraft and actuator state. Next, these dimensionless forces and moments are corrected for stall and then compressibility. The corrected aerodynamic coefficients are then used along with the aircraft propulsive force to determine the dimensional body-fixed forces and moments. The aircraft states are finally used with the calculated body-fixed forces and moments to determine the aircraft state and actuator dynamics.

A. Incompressible Aerodynamic Models

The wind coordinates aerodynamic force and body-fixed aerodynamic moment coefficients are determined using the aerodynamic model for the baseline aircraft developed in [5]

$$\mathring{C}_L = C_{L_1} + C_{L,\bar{q}}\bar{q} + C_{L,\delta_e}\delta_e \tag{8}$$

$$\mathring{C}_S = C_{S,\beta}\beta + (C_{S,L\bar{p}}C_{L_1} + C_{S,\bar{p}})\bar{p} + C_{S,\bar{r}}\bar{r} + C_{S,\delta_a}\delta_a + C_{S,\delta_r}\delta_r \tag{9}$$

$$\begin{aligned}\mathring{C}_D = {} & C_{D_0} + C_{D,L}C_{L_1} + C_{D,L^2}C_{L_1}^2 + C_{D,S^2}C_{S_1}^2 \\ & + C_{D,S\bar{p}}C_{S_1}\bar{p} + \left(C_{D,L^2\bar{q}}C_{L_1}^2 + C_{D,L\bar{q}}C_{L_1} + C_{D,\bar{q}}\right)\bar{q} + C_{D,S\bar{r}}C_{S_1}\bar{r} \\ & + C_{D,S\delta_a}C_{S_1}\delta_a + \left(C_{D,L\delta_e}C_{L_1} + C_{D,\delta_e}\right)\delta_e + C_{D,\delta_e^2}\delta_e^2 + C_{D,S\delta_r}C_{S_1}\delta_r\end{aligned} \tag{10}$$

$$\mathring{C}_\ell = C_{\ell,\beta}\beta + C_{\ell,\bar{p}}\bar{p} + (C_{\ell,L\bar{r}}C_{L_1} + C_{\ell,\bar{r}})\bar{r} + C_{\ell,\delta_a}\delta_a + C_{\ell,\delta_r}\delta_r \tag{11}$$

$$\mathring{C}_m = C_{m_0} + C_{m,\alpha}\alpha + C_{m,\bar{q}}\bar{q} + C_{m,\delta_e}\delta_e \tag{12}$$

$$\mathring{C}_n = C_{n,\beta}\beta + (C_{n,L\bar{p}}C_{L_1} + C_{n,\bar{p}})\bar{p} + C_{n,\bar{r}}\bar{r} + (C_{n,L\delta_a}C_{L_1} + C_{n,\delta_a})\delta_a + C_{n,\delta_r}\delta_r \tag{13}$$

where

$$C_{L_1} \equiv C_{L_0} + C_{L,\alpha}\alpha \tag{14}$$

$$C_{S_1} \equiv C_{S,\beta}\beta \tag{15}$$

$$\bar{p} \equiv \frac{pb_w}{2V}, \quad \bar{q} \equiv \frac{q\bar{c}_w}{2V}, \quad \bar{r} \equiv \frac{rb_w}{2V} \tag{16}$$

from which are determined the incompressible coefficients for lift ($\mathring{C}_L$), side-force ($\mathring{C}_S$), drag ($\mathring{C}_D$), rolling moment ($\mathring{C}_\ell$), pitching moment ($\mathring{C}_m$), and yawing moment ($\mathring{C}_n$). Subscripts following a comma denote the force or moment derivative with respect to a given variable. For example, the term C_{ℓ,δ_a} indicates the change in C_ℓ with respect to δ_a, and the term $C_{D,L^2\bar{q}}$ indicates the change in the quadratic $C_{D,\bar{q}}$ term with respect to $C_{L_1}^2$. Truncated values for these coefficient derivatives are reported in Tables A.4 and A.5.

In the aerodynamic model for the BIRE aircraft each coefficient is a function of the BIRE angle and takes the form [5]

$$\hat{C} = A\sin(\omega\delta_B + \phi) + z \tag{17}$$

where A is amplitude, ω is frequency, ϕ is phase, and z is offset. The BIRE aerodynamic model is

$$\mathring{C}_L = \hat{C}_{L_1} + \hat{C}_{L,\beta}\beta + \hat{C}_{L,\bar{p}}\bar{p} + \hat{C}_{L,\bar{q}}\bar{q} + \hat{C}_{L,\bar{r}}\bar{r} + \hat{C}_{L,\delta_a}\delta_a + \hat{C}_{L,\delta_e^B}\delta_e^B \tag{18}$$

$$\mathring{C}_S = \hat{C}_{S_0} + \hat{C}_{S,\alpha}\alpha + \hat{C}_{S,\beta}\beta + \left(\hat{C}_{S,L\bar{p}}\hat{C}_{L_1} + \hat{C}_{S,\bar{p}}\right)\bar{p} + \hat{C}_{S,\bar{q}}\bar{q} + \hat{C}_{S,\bar{r}}\bar{r} + \hat{C}_{S,\delta_a}\delta_a + \hat{C}_{S,\delta_e^B}\delta_e^B \tag{19}$$

$$\begin{aligned}\mathring{C}_D = {} & \hat{C}_{D_0} + \hat{C}_{D,L}\hat{C}_{L_1} + \hat{C}_{D,L^2}\hat{C}_{L_1}^2 + \hat{C}_{D,S}\hat{C}_{S_1} + \hat{C}_{D,S^2}\hat{C}_{S_1}^2 \\ & + \left(\hat{C}_{D,S\bar{p}}\hat{C}_{S_1} + \hat{C}_{D,\bar{p}}\right)\bar{p} + \left(\hat{C}_{D,L^2\bar{q}}\hat{C}_{L_1}^2 + \hat{C}_{D,L\bar{q}}\hat{C}_{L_1} + \hat{C}_{D,\bar{q}}\right)\bar{q} + \left(\hat{C}_{D,S\bar{r}}\hat{C}_{S_1} + \hat{C}_{D,\bar{r}}\right)\bar{r} \\ & + \left(\hat{C}_{D,S\delta_a}\hat{C}_{S_1} + \hat{C}_{D,\delta_a}\right)\delta_a + \left(\hat{C}_{D,L\delta_e^B}\hat{C}_{L_1} + \hat{C}_{D,\delta_e^B}\right)\delta_e^B + \hat{C}_{D,\delta_e^{B\,2}}\delta_e^{B\,2}\end{aligned} \tag{20}$$

$$\mathring{C}_\ell = \hat{C}_{\ell_0} + \hat{C}_{\ell,\alpha}\alpha + \hat{C}_{\ell,\beta}\beta + \hat{C}_{\ell,\bar{p}}\bar{p} + \hat{C}_{\ell,\bar{q}}\bar{q} + \left(\hat{C}_{\ell,L\bar{r}}\hat{C}_{L_1} + \hat{C}_{\ell,\bar{r}}\right)\bar{r} + \hat{C}_{\ell,\delta_a}\delta_a + \hat{C}_{\ell,\delta_e^B}\delta_e^B \tag{21}$$

$$\mathring{C}_m = \hat{C}_{m_0} + \hat{C}_{m,\alpha}\alpha + \hat{C}_{m,\beta}\beta + \hat{C}_{m,\bar{p}}\bar{p} + \hat{C}_{m,\bar{q}}\bar{q} + \hat{C}_{m,\bar{r}}\bar{r} + \hat{C}_{m,\delta_a}\delta_a + \hat{C}_{m,\delta_e^B}\delta_e^B \tag{22}$$

$$\mathring{C}_n = \hat{C}_{n_0} + \hat{C}_{n,\alpha}\alpha + \hat{C}_{n,\beta}\beta + \left(\hat{C}_{n,L\bar{p}}\hat{C}_{L_1} + \hat{C}_{n,\bar{p}}\right)\bar{p} + \hat{C}_{n,\bar{q}}\bar{q} + \hat{C}_{n,\bar{r}}\bar{r} + \left(\hat{C}_{n,L\delta_a}\hat{C}_{L_1} + \hat{C}_{n,\delta_a}\right)\delta_a + \hat{C}_{n,\delta_e^B}\delta_e^B \tag{23}$$

where

$$\hat{C}_{L_1} \equiv \hat{C}_{L_0} + \hat{C}_{L,\alpha}\alpha \tag{24}$$

$$\hat{C}_{S_1} \equiv \hat{C}_{S_0} + \hat{C}_{S,\beta}\beta \tag{25}$$

where a $\hat{}$ indicates the term follows the format specified in Eq. (17). Truncated values for these coefficients are reported in Tables A.6 and A.7.

B. Simulation Stall Model

The incompressible aerodynamics for the baseline and BIRE aircraft are first corrected for stall. A simple longitudinal flat-plate stall model is applied, where the stall-corrected lift, drag, and pitching moment coefficients are determined over a sigmoid transition to a flat-plate stall model from the aircraft aerodynamic model given in Eqs. (8)–(15) for the baseline aircraft and in Eqs. (18)–(25) for the BIRE aircraft. The flat plate coefficients for lift [41, 42], drag, and pitching moment can be approximated as

$$C_{L\,\text{plate}} = 2\,\text{sign}\,\alpha\,\sin^2\alpha\cos\alpha \tag{26}$$

$$C_{D\,\text{plate}} = 2\sin^{3/2}|\alpha| \tag{27}$$

$$C_{m\,\text{plate}} = -0.8\sin\alpha \tag{28}$$

The sigmoid blending function can be found as [42]

$$\sigma = \frac{1 + e^{-M(\alpha-\alpha_b)} + e^{M(\alpha+\alpha_b)}}{\left[1 + e^{-M(\alpha-\alpha_b)}\right]\left[1 + e^{M(\alpha+\alpha_b)}\right]} \tag{29}$$

where a value of 7 is used for the blending rate parameter M, and a value of 45° is used for the stall-transition angle α_b. These values were selected to best match the baseline aircraft lift coefficient wind tunnel data reported in [39]. The blended values for the lift, drag, and pitching moment coefficients can be found as

$$\acute{C}_L = (1-\sigma)\mathring{C}_L + \sigma C_{L\,\text{plate}} \tag{30}$$

$$\acute{C}_D = (1-\sigma)\mathring{C}_D + \sigma C_{D\,\text{plate}} \tag{31}$$

$$\acute{C}_m = (1-\sigma)\mathring{C}_m + \sigma C_{m\,\text{plate}} \tag{32}$$

Note, the stall model is not applied to the lateral force and moments (i.e. $\acute{C}_S = \mathring{C}_S$, $\acute{C}_\ell = \mathring{C}_\ell$, $\acute{C}_n = \mathring{C}_n$). This stall model will be applied in the time domain simulations and neglected in the control design due to the minimal effect of the stall model on the aircraft dynamics at the trim condition.

C. Compressibility

Next, compressibility is included in the aerodynamic model as a correction factor on the aerodynamic forces and moments. The implemented correction was developed by Anderson [43], which for a force or moment coefficient $\acute{C}_A$ is

$$C_A = \frac{\acute{C}_A\cos\Lambda_{c/2}}{\sqrt{1 - M^2\cos^2\Lambda_{c/2} + \left[\frac{\acute{C}_A\cos\Lambda_{c/2}}{(\pi R_A)}\right]^2} + \frac{\acute{C}_A\cos\Lambda_{c/2}}{(\pi R_A)}} \tag{33}$$

where $\Lambda_{c/2}$ is the half-chord sweep angle and R_A the aspect ratio of the lifting surface primarily responsible for the incompressible force or moment coefficient $\mathring{C}_A$. Table 1 lists the values used in the correction factor for the baseline and BIRE aircraft, respectively. Note the drag coefficient is not adjusted for compressibility (i.e. $C_D = \acute{C}_D$).

Table 1 Compressibility correction values for each aircraft by force and moment, from Bolander [6].

	baseline			BIRE		
Coefficient	influencing surface	$\Lambda_{c/2}$ [°]	R_A	influencing surface	$\Lambda_{c/2}$ [°]	R_A
C_L	main wing	23	3	main wing	23	3
C_S	vertical stabilizer	38	1.29	horizontal stabilizer	22	2.116
C_ℓ	vertical stabilizer	38	1.29	main wing	23	3
C_m	main wing	23	3	main wing	23	3
C_n	vertical stabilizer	38	1.29	horizontal stabilizer	22	2.116

D. Thrust Model

Both the baseline and BIRE aircraft share the propulsion model previously developed by Bolander [6]. The thrust can be found using the engine percent power, given by Nguyen et al. [39] and Stevens and Lewis [7], as

$$P_1 = \begin{cases} 64.94\tau, & \tau \leq 0.77 \\ 217.38\tau - 117.38, & \tau > 0.77 \end{cases} \tag{34}$$

The percent power P_1 is converted to total thrust as [6, 7, 39]

$$T = \begin{cases} T_{\text{idle}} + (T_{\text{mil}} - T_{\text{idle}})\frac{P_1}{50}, & P_1 < 50 \\ T_{\text{mil}} + (T_{\text{max}} - T_{\text{mil}})\frac{P_1 - 50}{50}, & P_1 \geq 50 \end{cases} \tag{35}$$

The idle-, mil-, and max-setting total thrust values can be found from the the thrust model

$$T_{\text{set}} = \left(\frac{\rho}{\rho_0}\right)^{a_{\text{set}}} \left(T_{\text{set}\,0} + T_{\text{set}\,1} V + T_{\text{set}\,2} V^2\right) \tag{36}$$

where the coefficients a_{set}, $T_{\text{set}\,0}$, $T_{\text{set}\,1}$, and $T_{\text{set}\,2}$ can be found from the fits developed by Bolander [6] for each setting as

$$T_{\text{set}\,i} = c_{\text{set}\,0} + c_{\text{set}\,1} H + c_{\text{set}\,2} H^2 \tag{37}$$

and the individual fit coefficients are given in Table 2.

Table 2 Thrust model fit coefficients [6].

	Coefficient	T_{idle}	T_{mil}	T_{max}
a	c_0	1.0104	1.0148	1.0225
	$c_1 \times 10^5$	2.9484	3.1355	3.1984
	$c_2 \times 10^{10}$	-3.8270	-4.2106	-4.3617
T_0	c_0 [lbf]	3145	11716	20341
	c_1 [lbf ft]	-0.4185	0.1156	0.1454
	$c_2 \times 10^5$ [lbf ft^2]	1.8313	0.3474	0.9283
T_1	c_0 [lbf ft / s]	-4.3491	3.5689	1.9886
	$c_1 \times 10^4$ [lbf ft^2 / s]	-4.9703	0.1409	6.3926
	$c_2 \times 10^8$ [lbf ft^3 / s]	1.3557	-0.3982	-2.4428
T_2	$c_0 \times 10^3$ [lbf ft^2 / s^2]	-0.2321	-3.9793	3.5201
	$c_1 \times 10^7$ [lbf ft^3 / s^2]	5.5629	2.6931	0.7574
	$c_2 \times 10^{11}$ [lbf ft^4 / s^2]	-2.0550	0.5281	2.6665

E. Body-Fixed Aerodynamic Forces and Moments

Assuming the thrust to be aligned with the x-axis and located at the center of gravity, the body-fixed aerodynamic and thrust forces (F_{x_b},F_{y_b},F_{z_b}) and moments (M_{x_b},M_{y_b},M_{z_b}) can be found as

$$\begin{bmatrix} F_{x_b} \\ F_{y_b} \\ F_{z_b} \end{bmatrix} = \frac{1}{2}\rho V^2 S_w \begin{bmatrix} C_L S_\alpha - C_S C_\alpha S_\beta - C_D C_\alpha C_\beta \\ C_S C_\beta - C_D S_\beta \\ -C_L C_\alpha - C_S S_\alpha S_\beta - C_D S_\alpha C_\beta \end{bmatrix} + \begin{bmatrix} T \\ 0 \\ 0 \end{bmatrix} \tag{38}$$

$$\begin{bmatrix} M_{x_b} \\ M_{y_b} \\ M_{z_b} \end{bmatrix} = \frac{1}{2}\rho V^2 S_w \begin{bmatrix} b_w C_\ell \\ \bar{c}_w C_m \\ b_w C_n \end{bmatrix} \tag{39}$$

F. Equations of Motion

The aircraft EOM are used to determine the time rate-of-change of the aircraft states. The differential equations governing aircraft motion are given in Eq. (40). The EOM depend on the aircraft state and aerodynamic forces and moments, as well as the moments and products of inertia (I_{xx_b},I_{yy_b},I_{zz_b} and I_{xy_b},I_{xz_b},I_{yz_b}), and angular momentum (h_{x_b},h_{y_b},h_{z_b}). Note, C_χ and S_χ indicate the cosine or sine of an angle χ, respectively.

$$\begin{bmatrix} \dot{V}_{x_b} \\ \dot{V}_{y_b} \\ \dot{V}_{z_b} \end{bmatrix} = \frac{g}{W} \begin{bmatrix} F_{x_b} \\ F_{y_b} \\ F_{z_b} \end{bmatrix} + g \begin{bmatrix} -S_\theta \\ S_\phi C_\theta \\ C_\phi C_\theta \end{bmatrix} + \begin{bmatrix} rV_{y_b} - qV_{z_b} \\ pV_{z_b} - rV_{x_b} \\ qV_{x_b} - pV_{y_b} \end{bmatrix}$$

$$\begin{bmatrix} \dot{p} \\ \dot{q} \\ \dot{r} \end{bmatrix} = \begin{bmatrix} I_{xx_b} & -I_{xy_b} & -I_{xz_b} \\ -I_{xy_b} & I_{yy_b} & -I_{yz_b} \\ -I_{xz_b} & -I_{yz_b} & I_{zz_b} \end{bmatrix}^{-1} \left[\begin{bmatrix} M_{x_b} \\ M_{y_b} \\ M_{z_b} \end{bmatrix} + \begin{bmatrix} 0 & -h_{z_b} & h_{y_b} \\ h_{z_b} & 0 & -h_{x_b} \\ -h_{y_b} & h_{x_b} & 0 \end{bmatrix} \begin{bmatrix} p \\ q \\ r \end{bmatrix} + \begin{bmatrix} (I_{yy_b} - I_{zz_b})qr + I_{yz_b}(q^2 - r^2) + I_{xz_b}pq - I_{xy_b}pr \\ (I_{zz_b} - I_{xx_b})pr + I_{xz_b}(r^2 - p^2) + I_{xy_b}qr - I_{yz_b}pq \\ (I_{xx_b} - I_{yy_b})pq + I_{xy_b}(p^2 - q^2) + I_{yz_b}pr - I_{xz_b}qr \end{bmatrix} \right] \tag{40}$$

$$\begin{bmatrix} \dot{x}_f \\ \dot{y}_f \\ \dot{z}_f \end{bmatrix} = \begin{bmatrix} C_\theta C_\psi & S_\phi S_\theta C_\psi - C_\phi S_\psi & C_\phi S_\theta C_\psi + S_\phi S_\psi \\ C_\theta S_\psi & S_\phi S_\theta S_\psi + C_\phi C_\psi & C_\phi S_\theta S_\psi - S_\phi C_\psi \\ -S_\theta & S_\phi C_\theta & C_\phi C_\theta \end{bmatrix} \begin{bmatrix} V_{x_b} \\ V_{y_b} \\ V_{z_b} \end{bmatrix}$$

$$\begin{bmatrix} \dot{\phi} \\ \dot{\theta} \\ \dot{\psi} \end{bmatrix} = \begin{bmatrix} 1 & S_\phi S_\theta / C_\theta & C_\phi S_\theta / C_\theta \\ 0 & C_\phi & -S_\phi \\ 0 & S_\phi / C_\theta & C_\phi / C_\theta \end{bmatrix} \begin{bmatrix} p \\ q \\ r \end{bmatrix}$$

Equations (4)–(40) can be summarized as

$$\dot{x} = f(x, \delta) \tag{41}$$

G. Actuator Dynamics

The implemented first-order actuator model is

$$\dot{\delta}_i = \sigma_i \left(u_i - \delta_i \right) \tag{42}$$

for commanded input u_i and actuator state δ_i with gain σ_i. The actuation rates model is thus applied as

$$\dot{\delta} = \begin{bmatrix} \dot{\delta}_a \\ \dot{\delta}_e \\ \dot{\delta}_r \\ \dot{\tau} \end{bmatrix} = \Upsilon \left(u - \delta \right) = \begin{bmatrix} \sigma_{\delta_a} & 0 & 0 & 0 \\ 0 & \sigma_{\delta_e} & 0 & 0 \\ 0 & 0 & \sigma_{\delta_r} & 0 \\ 0 & 0 & 0 & \sigma_\tau \end{bmatrix} \left(\begin{bmatrix} \delta_{a,\,cmd} \\ \delta_{e,\,cmd} \\ \delta_{r,\,cmd} \\ \tau_{cmd} \end{bmatrix} - \begin{bmatrix} \delta_a \\ \delta_e \\ \delta_r \\ \tau \end{bmatrix} \right) \tag{43}$$

or in the case of the BIRE,

$$\dot{\delta} = \begin{bmatrix} \dot{\delta}_a \\ \dot{\delta}_e^B \\ \dot{\delta}_B \\ \dot{\tau} \end{bmatrix} = \Upsilon\left(u - \delta\right) = \begin{bmatrix} \sigma_{\delta_a} & 0 & 0 & 0 \\ 0 & \sigma_{\delta_e^B} & 0 & 0 \\ 0 & 0 & \sigma_{\delta_B} & 0 \\ 0 & 0 & 0 & \sigma_\tau \end{bmatrix} \left(\begin{bmatrix} \delta_{a,\,cmd} \\ \delta^B_{e,\,cmd} \\ \delta_{B,\,cmd} \\ \tau_{cmd} \end{bmatrix} - \begin{bmatrix} \delta_a \\ \delta_e^B \\ \delta_B \\ \tau \end{bmatrix} \right) \tag{44}$$

The first-order lag values reported by Nguyen et al. used in the actuator model are given in Table 3. Note, the values for the BIRE actuator were estimated based on the first-order lag of the other control effectors and preliminary mechanical analyses.

Table 3 Actuation rates and limits for control surfaces on the baseline and BIRE aircraft [39].

Input	δ_a	δ_e	δ_r	δ_B	τ
First-Order Lag [s] $(1/\sigma_i)$	0.0495	0.0495	0.0495	0.0495	$\begin{cases} 1.0, & \tau < 0.3 \\ 1\,/(2.35 - 4.5\tau)\,, & 0.3 \le \tau < 0.5 \\ 10.0, & \tau \ge 0.5 \end{cases}$
Input Limit $(\delta_{i\,max})$	± 21.5°	± 25°	± 30°	± 90°	[0 1]
Actuation Rate Limit $(\dot{\delta}_{i\,max})$	± 80°/s	± 60°/s	± 120°/s	± 50°/s	-

The system in Eq. (43) for the baseline or Eq. (44) for the BIRE can be summarized as

$$\dot{\delta} = g(\delta, u) \tag{45}$$

H. Aggregate System

The aircraft and actuator states can be aggregated as

$$z = \begin{bmatrix} x \\ \delta \end{bmatrix} \tag{46}$$

and used to form the full aggregated nonlinear dynamics as

$$\dot{z} = \begin{bmatrix} \dot{x} \\ \dot{\delta} \end{bmatrix} = h(z, u) = \begin{bmatrix} f(x, \delta) \\ g(\delta, u) \end{bmatrix} \tag{47}$$

I. Disturbances and Uncertainties

A disturbance model was implemented in the present work for introducing turbulence into the aircraft aerodynamic model. This disturbance model is an implementation of the von Kármán atmospheric turbulence model. The model was developed using the von Kármán turbulence velocity spectra [44, 45] and Department of Defense recommended angular rates spectra [44] using the sum-of-sines method outlined by Beal [45]. The disturbance in V_{x_b}, V_{y_b}, V_{z_b}, p, q, and r were each found as a sum of sines. For example, the body-fixed disturbance x_b-velocity is computed as

$$V_{x_b\,turb} = A_{x_b\,turb} \sum_{i=0}^{n} \sin\left(\omega_i x_k + \phi_i\right) \tag{48}$$

where ω_i represents the individual frequencies, ϕ_i represents the individual random phases, and $A_{x_b\,turb}$ is the signal amplitude. The spatial coordinate x_k was determined as a $x_k = V_k t_k$, where k denotes a discretized time in simulation. These disturbances were combined with the state at time t_k to determine aerodynamic forces and moments from Eqs. (8)–(15) for the baseline and from Eqs. (18)–(25) for the BIRE.

This sum-of-sines process assumes the turbulent flow field to be frozen in space. The method presented by Beal entails dividing the velocity and angular rate spectral densities into equal area sections. The central frequency of each

area, with fixed amplitudes (determined from the area of each section) and uniformly random phase shifts for each sine wave, is used to form the summed sine waves defining the atmospheric noise. This turbulence model primarily depends on the aircraft altitude, an integer number of frequencies for the sum-of-sines method, and a turbulence intensity setting (trim altitude, 100, and `light`, respectively, unless otherwise specified).

In addition to a turbulence model, an uncertainty model was implemented to evaluate system response to uncertainty in the aerodynamic forces and moments. This error was applied multiplicatively, shown on the lift coefficient as

$$C_L = \left(1 + \epsilon_{C_L}\right) C_{L\,\text{true}} \tag{49}$$

where the dimensionless errors ϵ_{C_A} were selected for each force or moment coefficient C_A from a random normal distribution as a fixed value during each simulation. This error was applied to the aerodynamic forces and moments coefficients immediately after they were corrected for compressibility. Note, an individual error could have been applied to each of the coefficients in the aerodynamic models in Eqs. (8)–(15) and Eqs. (18)–(25) as well as the weight, inertia, gyroscopic terms, and center of gravity location. However, it would be extremely difficult to summarize or state much about the resulting analyses, due to the expansiveness of the stochastic variables and the requisite number of simulation runs. Simulations performed by the authors showed that similar responses of the forces and moments of the aircraft compared to the application of individual coefficient errors could be achieved by simply adding the multiplicative error presented. For these reasons the multiplicative error was chosen as the aerodynamic model error implementation. The effects of turbulence and model error are discussed in the controller performance results presented later.

III. Linearized Model and Properties

The nonlinear system given in Eq. (47) is linearized as a first step in developing the linear controller. This linearization is performed in Appendix B. Note that the actuator dynamics are excluded from the control design. Thus, the controller is designed for the system

$$\dot{x} = f(x, u) \tag{50}$$

The use of the function f denotes the same dynamics as indicated in Eq. (41) with merely a change in the input to the system (commanded control u replacing actuator states δ).

A. Linearized System

In the control design of the linearized system only a portion of the state will be fed back, which is

$$\begin{aligned}
\Delta x &= \begin{bmatrix}
1 & 0 & 0 & 0 & 0 & 0 & 0 & 0 & 0 & 0 & 0 & 0 \\
0 & 1 & 0 & 0 & 0 & 0 & 0 & 0 & 0 & 0 & 0 & 0 \\
0 & 0 & 1 & 0 & 0 & 0 & 0 & 0 & 0 & 0 & 0 & 0 \\
0 & 0 & 0 & 1 & 0 & 0 & 0 & 0 & 0 & 0 & 0 & 0 \\
0 & 0 & 0 & 0 & 1 & 0 & 0 & 0 & 0 & 0 & 0 & 0 \\
0 & 0 & 0 & 0 & 0 & 1 & 0 & 0 & 0 & 0 & 0 & 0 \\
0 & 0 & 0 & 0 & 0 & 0 & 0 & 0 & 1 & 0 & 0 & 0 \\
0 & 0 & 0 & 0 & 0 & 0 & 0 & 0 & 0 & 1 & 0 & 0 \\
0 & 0 & 0 & 0 & 0 & 0 & 0 & 0 & 0 & 0 & 1 & 0
\end{bmatrix} (x - x_{tr}) = C\,(x - x_{tr}) \\
\Delta u &= u - u_{tr}
\end{aligned} \tag{51}$$

The terms Δx and Δu denote the difference in the linearized state and control from the trim state and control (x_{tr}, and u_{tr}), respectively. The C matrix as we have defined it reduces the state, removing the x_f, y_f, and ψ states. These states are removed because they have no effect on the trim condition of the aircraft (due to the flat-Earth EOM in Eq. (40)). The system in Eq. (50) can be linearized following the process outlined in Appendix B to form the linear system

$$\Delta\dot{x} = A|_{(x_{tr},u_{tr})}\,\Delta x + B|_{(x_{tr},u_{tr})}\,\Delta u \tag{52}$$

where the state matrix A is given symbolically in (B.180) and control matrix B is given symbolically in (B.199). In order to evaluate the linearized system matrices a trim state and control must be found such that

$$\dot{x} = f(x_{tr}, u_{tr}) = 0 \tag{53}$$

In this work a trim algorithm is used to numerically determine x_{tr} and u_{tr} (note $\delta_{tr} = u_{tr}$) as outlined in [6] using the Newton-Raphson method [46].

B. Numerical Models at the Air Combat Maneuver Condition Trim Point

The system given in (52) can be evaluated at the Air Combat Maneuver Condition [6, 47, 48] (15,000 ft altitude above sea level, Mach number 0.6, steady level flight). The trim condition for the baseline at the Air Combat Maneuver Condition is

$$x_{tr} = \begin{bmatrix} 633.7185 \\ 0 \\ 29.6840 \\ -0 \\ 0 \\ 0 \\ 0 \\ 0 \\ -15000 \\ 0 \\ 0.0468 \\ 0 \end{bmatrix}, \quad \delta_{tr} = \begin{bmatrix} 0 \\ -0.0030 \\ 0 \\ 0.2772 \end{bmatrix}, \quad u_{tr} = \begin{bmatrix} 0 \\ -0.0030 \\ 0 \\ 0.2772 \end{bmatrix} \tag{54}$$

which results in the state and control matrices (recall the states x_f, y_f, and ψ have been removed from this matrix, as shown in Eqs. (B.180) and (B.199))

$$A = \begin{bmatrix} -0.0056 & 0 & 0.0548 & 0 & -29.7176 & 0 & 0 & 0 & -32.0926 \\ 0 & -0.1848 & 0 & 29.8499 & 0 & -632.4144 & 0 & 32.0926 & 0 \\ -0.1340 & 0 & -0.8499 & 0 & 629.2103 & 0 & 0 & 0 & -1.5033 \\ 0 & -0.0301 & 0 & -1.9238 & 0.0003 & 0.4041 & 0 & 0 & 0 \\ -0.0003 & 0 & 0.0056 & 0 & -0.8753 & -0.0029 & 0 & 0 & 0 \\ 0 & 0.0142 & 0 & -0.0375 & 0.0025 & -0.1560 & 0 & 0 & 0 \\ -0.0468 & 0 & 0.9989 & 0 & 0 & 0 & 0 & 0 & -634.4133 \\ 0 & 0 & 0 & 1 & 0 & 0.0468 & 0 & 0 & 0 \\ 0 & 0 & 0 & 0 & 1 & 0 & 0 & 0 & 0 \end{bmatrix} \tag{55}$$

$$B = \begin{bmatrix} 0 & -0.7212 & 0 & 21.1331 \\ 8.3046 & 0 & 21.4957 & 0 \\ 0 & -84.2119 & 0 & 0 \\ -19.0435 & 0 & 6.2114 & 0 \\ 0 & -11.8963 & 0 & 0 \\ -1.2933 & 0 & -3.3559 & 0 \\ 0 & 0 & 0 & 0 \\ 0 & 0 & 0 & 0 \\ 0 & 0 & 0 & 0 \end{bmatrix} \tag{56}$$

The trim condition for the BIRE at the same condition (15,000 ft altitude above sea level, Mach number 0.6, steady level flight) is

$$x_{tr} = \begin{bmatrix} 633.7375 \\ 0 \\ 29.2742 \\ -0 \\ 0 \\ 0 \\ 0 \\ 0 \\ -15000 \\ 0 \\ 0.0462 \\ 0 \end{bmatrix}, \quad \delta_{tr} = \begin{bmatrix} 0 \\ 0.0007 \\ 0 \\ 0.2732 \end{bmatrix}, \quad u_{tr} = \begin{bmatrix} 0 \\ 0.0007 \\ 0 \\ 0.2732 \end{bmatrix} \tag{57}$$

At this trim condition the BIRE requires slightly less throttle command, due ot the lack of drag produced by a vertical tail. Evaluating the A and B matrices at the trim state and control in Eq. (57) results in the state and control matrices (recall the states x_f, y_f, and ψ have been removed from this matrix, as shown in Eqs. (B.180) and (B.199))

$$A = \begin{bmatrix} -0.0051 & -0.0000 & 0.0529 & 0 & -29.2933 & 0 & 0 & 0 & -32.0936 \\ 0 & -0.0458 & 0 & 29.4573 & 0 & -633.7953 & 0 & 32.0936 & 0 \\ -0.1347 & -0.0000 & -0.8463 & 0 & 629.1079 & 0 & 0 & 0 & -1.4825 \\ 0 & -0.0135 & -0.0000 & -2.3097 & -0.0000 & 0.2295 & 0 & 0 & 0 \\ -0.0002 & -0.0000 & 0.0041 & -0.0000 & -0.8493 & -0.0027 & 0 & 0 & 0 \\ -0.0000 & -0.0027 & 0 & -0.0151 & 0.0004 & 0.0114 & 0 & 0 & 0 \\ -0.0461 & 0 & 0.9989 & 0 & 0 & 0 & 0 & 0 & -634.4133 \\ 0 & 0 & 0 & 1 & 0 & 0.0462 & 0 & 0 & 0 \\ 0 & 0 & 0 & 0 & 1 & 0 & 0 & 0 & 0 \end{bmatrix} \tag{58}$$

$$B = \begin{bmatrix} -0.0044 & -0.9987 & -0.0000 & 20.6299 \\ -7.8524 & 0 & -0.5816 & 0 \\ 0.0957 & -84.6130 & -0.0000 & 0 \\ -29.8253 & 0 & -0.0129 & 0 \\ -0.0104 & -12.0443 & 0.0001 & 0 \\ 0.8468 & -0.0294 & 0.0381 & 0 \\ 0 & 0 & 0 & 0 \\ 0 & 0 & 0 & 0 \\ 0 & 0 & 0 & 0 \end{bmatrix} \tag{59}$$

For small BIRE angles (as shown in Eq. (59)) the B matrix is lightly coupled between longitudinal and lateral dynamics. This coupling increases significantly for larger BIRE angles ($\delta_B > 10^\circ$), prohibiting control design using traditional uncoupled techniques. Note the ailerons are the main yaw control effector for the BIRE aircraft.

C. Controllability

The controllability of each aircraft system was evaluated at the Air Combat Maneuver Condition at various steady coordinated turn trim bank angles (note for a steady coordinated non-climbing turn $\phi_{tr} = 0$ results in steady level flight). The controllability matrix and corresponding rank were found for both the baseline and BIRE aircraft. Each controllability matrix was full rank, and thus each linearized aircraft is controllable at the Air Combat Maneuver Condition.

D. Open-Loop Modes

The open-loop modes of each aircraft can be evaluated by finding the eigenvalues λ_{ol} of the baseline A matrix given in Eq. (55), which are

$$\lambda_{ol} = \begin{bmatrix} 0 + 0j \\ -0.1758 + 3.1455j \\ -0.1758 - 3.1455j \\ -1.9170 + 0j \\ -2.7439 + 0j \\ 1.0300 + 0j \\ 0.0040 + 0j \\ -0.0085 + 0.1050j \\ -0.0085 - 0.1050j \end{bmatrix} \tag{60}$$

which correspond to the eigenvectors

$$\chi_{ol} = \left\{ \begin{bmatrix} 0 + 0j \\ 0 + 0j \\ 0 + 0j \\ 0 + 0j \\ 0 + 0j \\ 0 + 0j \\ 1 + 0j \\ 0 + 0j \\ 0 + 0j \end{bmatrix}, \begin{bmatrix} -0 + 0j \\ 1.0000 + 0j \\ 0.0002 - 0.0006j \\ -0.0045 + 0.0071j \\ 0 + 0j \\ -0.0001 - 0.0046j \\ 0 - 0.0001j \\ 0.0023 + 0.0013j \\ 0 - 0.0000j \end{bmatrix}, \begin{bmatrix} -0 - 0.0000j \\ 1.0000 - 0j \\ 0.0002 + 0.0006j \\ -0.0045 - 0.0071j \\ 0 - 0.0000j \\ -0.0001 + 0.0046j \\ 0 + 0.0001j \\ 0.0023 - 0.0013j \\ 0 + 0j \end{bmatrix}, \begin{bmatrix} 0.0006 + 0j \\ -0.0481 + 0j \\ -0.0137 + 0j \\ -0.8852 + 0j \\ 0 + 0j \\ -0.0185 + 0j \\ 0.0031 + 0j \\ 0.4622 + 0j \\ -0 + 0j \end{bmatrix}, \begin{bmatrix} 0.0396 + 0j \\ -0.0003 + 0j \\ -0.9932 + 0j \\ -0 + 0j \\ 0.0030 + 0j \\ -0 + 0j \\ 0.1098 + 0j \\ 0 + 0j \\ -0.0011 + 0j \end{bmatrix}, \right.$$

$$\left. \begin{bmatrix} 0.0945 + 0j \\ 0.0003 + 0j \\ -0.7774 + 0j \\ -0 + 0j \\ -0.0023 + 0j \\ -0 + 0j \\ 0.6219 + 0j \\ -0 + 0j \\ -0.0022 + 0j \end{bmatrix}, \begin{bmatrix} 0.0252 + 0j \\ -0.1142 + 0j \\ -0.0040 + 0j \\ -0.0003 + 0j \\ -0 + 0j \\ -0.0101 + 0j \\ 0.9730 + 0j \\ -0.1989 + 0j \\ -0 + 0j \end{bmatrix}, \begin{bmatrix} 0.0500 + 0.0062j \\ -0 - 0.0000j \\ 0.0049 + 0.0011j \\ 0 + 0j \\ 0 + 0j \\ 0 - 0.0000j \\ 0.9987 + 0j \\ 0 - 0.0000j \\ 0 - 0.0002j \end{bmatrix}, \begin{bmatrix} 0.0500 - 0.0062j \\ -0 + 0j \\ 0.0049 - 0.0011j \\ 0 - 0.0000j \\ 0 - 0.0000j \\ 0 + 0j \\ 0.9987 - 0j \\ 0 + 0j \\ 0 + 0.0002j \end{bmatrix} \right\} \tag{61}$$

The eigenvectors can be used to identify [49, 50] the dynamic modes of the aircraft, along with corresponding handling qualities (HQ). The open-loop modes and corresponding HQ are given in Table 4. The HQ levels are assigned from the limits established in MIL-F-8785C [51] and summarized by Hodgkinson [52] and Phillips [53] for class IV aircraft in flight phase A (the constraining limits for this highly-maneuverable fighter and BIRE variant).

Table 4 Baseline aircraft open-loop modes and HQ levels.

$\lambda_{ol\,i}$	Mode	σ [1/s]	ω_n [rad/s]	ζ	CAP [s^{-2}]	t_{db} [s]	t_c [s]	HQ
$0+0j$	rigid-body	-0.000	-	-	-	-	-	-
$-0.1758+3.1455j$	Dutch roll	0.176	3.150	0.056	-	-	-	Level 2
$-0.1758-3.1455j$	Dutch roll	0.176	3.150	0.056	-	-	-	Level 2
$-1.9170+0j$	roll	1.917	-	-	-	-	0.522	Level 1
$-2.7439+0j$	short period	2.744	-	-	-	-	0.364	Level 4
$1.0300+0j$	short period	-1.030	-	-	-	0.673	-	Level 4
$0.0040+0j$	spiral	-0.004	-	-	-	172.937	-	Level 1
$-0.0085+0.1050j$	phugoid	0.009	0.105	0.081	-	-	-	Level 1
$-0.0085-0.1050j$	phugoid	0.009	0.105	0.081	-	-	-	Level 1

The rigid-body mode is trivial, and denotes that the aircraft can be flown in steady level flight at different altitudes [49], and will not be discussed further in the present paper. As shown in Table 4 the baseline has particularly poor handling qualities for the Dutch roll and short period modes. The Dutch roll mode has insufficient damping, and the short period mode is unstable.

The eigenvalues of the BIRE A matrix given in Eq. (58) are

$$\lambda_{ol} = \begin{bmatrix} 0+0j \\ -2.2074+0j \\ -2.4526+0j \\ -1.3113+0j \\ 1.1675+0j \\ 0.7722+0j \\ 0.0071+0j \\ -0.0101+0.1093j \\ -0.0101-0.1093j \end{bmatrix} \tag{62}$$

which correspond to the eigenvectors

$$\chi_{ol} = \left\{ \begin{bmatrix} 0+0j \\ 0+0j \\ 0+0j \\ 0+0j \\ 0+0j \\ 0+0j \\ 1+0j \\ 0+0j \\ 0+0j \end{bmatrix}, \begin{bmatrix} -0.0001+0j \\ 0.9898+0j \\ 0.0025+0j \\ -0.1297+0j \\ -0+0j \\ 0.0003+0j \\ -0.0004+0j \\ 0.0587+0j \\ 0+0j \end{bmatrix}, \begin{bmatrix} 0.0382+0j \\ 0.0008+0j \\ -0.9899+0j \\ 0.0001+0j \\ 0.0025+0j \\ 0+0j \\ 0.1367+0j \\ -0+0j \\ -0.0010+0j \end{bmatrix}, \begin{bmatrix} -0.0001+0j \\ 0.9999+0j \\ 0.0032+0j \\ -0.0131+0j \\ -0+0j \\ 0.0019+0j \\ -0.0016+0j \\ 0.0099+0j \\ 0+0j \end{bmatrix}, \begin{bmatrix} -0.0001+0j \\ -1.0000+0j \\ 0.0005+0j \\ 0.0040+0j \\ 0+0j \\ 0.0023+0j \\ -0.0003+0j \\ 0.0035+0j \\ 0+0j \end{bmatrix} \right\},$$

$$\left\{ \begin{bmatrix} -0.0947 + 0j \\ 0.0050 + 0j \\ 0.5773 + 0j \\ -0 + 0j \\ 0.0015 + 0j \\ -0 + 0j \\ -0.8110 + 0j \\ -0 + 0j \\ 0.0019 + 0j \end{bmatrix}, \begin{bmatrix} 0.0347 + 0j \\ -0.0115 + 0j \\ -0.0056 + 0j \\ -0.0010 + 0j \\ -0 + 0j \\ -0.0107 + 0j \\ 0.9769 + 0j \\ -0.2101 + 0j \\ -0 + 0j \end{bmatrix}, \begin{bmatrix} 0.0499 + 0.0061j \\ 0 + 0j \\ 0.0060 + 0.0016j \\ -0 - 0.0000j \\ 0 + 0j \\ -0 + 0j \\ 0.9987 + 0j \\ -0 + 0j \\ 0 - 0.0002j \end{bmatrix}, \begin{bmatrix} 0.0499 - 0.0061j \\ 0 - 0.0000j \\ 0.0060 - 0.0016j \\ -0 + 0j \\ 0 - 0.0000j \\ -0 - 0.0000j \\ 0.9987 - 0j \\ -0 - 0.0000j \\ 0 + 0.0002j \end{bmatrix} \right\} \tag{63}$$

The eigenvalues can be used to identify the dynamic modes of the aircraft, along with corresponding HQ. The open-loop modes and corresponding HQ are given in Table 5 (using the same limits as evaluated on the baseline aircraft).

Table 5 BIRE aircraft open-loop modes and HQ levels.

$\lambda_{ol\,i}$	Mode	σ [1/s]	ω_n [rad/s]	ζ	CAP [s^{-2}]	t_{db} [s]	t_c [s]	HQ
$0 + 0j$	rigid-body	-0.000	-	-	-	-	-	-
$-2.2074 + 0j$	roll	2.207	-	-	-	-	0.453	Level 1
$-2.4526 + 0j$	short period	2.453	-	-	-	-	0.408	Level 4
$-1.3113 + 0j$	Dutch roll	1.311	-	-	-	-	0.763	Level 4
$1.1675 + 0j$	Dutch roll	-1.168	-	-	-	0.594	-	Level 4
$0.7722 + 0j$	short period	-0.772	-	-	-	0.898	-	Level 4
$0.0071 + 0j$	spiral	-0.007	-	-	-	98.088	-	Level 1
$-0.0101 + 0.1093j$	phugoid	0.010	0.110	0.092	-	-	-	Level 1
$-0.0101 - 0.1093j$	phugoid	0.010	0.110	0.092	-	-	-	Level 1

As shown in Table 5 the BIRE, like the baseline, has particularly poor handling qualities for the Dutch roll and short period modes. Both the Dutch roll and the short period modes are unstable. Though the baseline and BIRE are analyzed at near identical trim conditions, and (as the BIRE is undeflected) have near identical aerodynamics, significant differences arise in the comparison of the corresponding dynamic modes of the two aircraft. As the BIRE does not have a vertical tail, the spiral mode time to double and Dutch roll handling quality are worse than those of the baseline aircraft. Also, the phugoid damping of the BIRE aircraft is slightly higher than that of the baseline aircraft. This effect may stem from the lack of anhedral on the BIRE stabilators (and thus increased effective longitudinal stabilizing surface area).

The high instability in the baseline short period and BIRE short period and Dutch roll modes demonstrate the need for a stabilizing controller. A stabilizing controller can augment the natural stability of the aircraft such that the pilot is agnostic to the aircraft unstable modes. The short period and Dutch roll modes depend heavily on the aircraft body-fixed rotation rates. Thus, a first step in the control design would be to heavily weight the relative importance of these rotation rates. The aircraft orientation also plays a significant role in these modes, and should carry greater weight in the control design. The control design for the baseline aircraft has been studied extensively [24–33, 36–38], and as such is neglected in the present paper. Only the control design for the BIRE is presented with performance analysis.

IV. Control Design

A stabilizing controller can be designed to mitigate the handling deficiencies given in Table 5 for the BIRE. Such a design should not only improve the aircraft HQ, but also be robust to error and disturbance.

A. LQR Design

The objective of the infinite-horizon LQR optimal-control problem is to minimize the cost function

$$J = \int_0^\infty \left(\Delta x^T Q \Delta x + \Delta u^T R \Delta u \right) dt \tag{64}$$

This is done by solving the algebraic Riccati equation

$$0 = A^T P + PA + Q - PBR^{-1}B^T P \tag{65}$$

for the positive semidefinite matrix P to find an optimal control policy

$$\Delta u = -\left(R^{-1}B^T P\right)\Delta x = -K\Delta x \tag{66}$$

where K is the state feedback gain matrix. Inserting Eq. (51) and rearranging, the optimal control policy is

$$u = u_{tr} - K\Delta x \tag{67}$$

State and control weighting matrices that result in quality performance metrics for the BIRE aircraft are

$$Q = \text{diag}\left(\begin{bmatrix} 1e^{-6} \\ 1e^{-6} \\ 1e^{-6} \\ 1 \\ 1 \\ 1 \\ 1e^{-6} \\ 1 \\ 1 \end{bmatrix}\right), \quad R = \text{diag}\left(\begin{bmatrix} 5 \\ 5 \\ 5 \\ 5e^{-2} \end{bmatrix}\right) \tag{68}$$

which with the state and input matrices in Eqs. (58)–(59) are used to calculate the state feedback gain matrix

$$K = \begin{bmatrix} -0.0000 & -0.0208 & 0 & -0.2127 & -0.0208 & 9.8456 & 0 & -0.0607 & -0.0363 \\ -0.0002 & 0.0003 & 0.0001 & -0.0029 & -0.5341 & -0.1542 & 0.0004 & -0.0059 & -1.0029 \\ -0.0000 & -0.0030 & 0 & 0.0275 & -0.0029 & 1.3998 & 0 & 0.0545 & -0.0051 \\ 0.0047 & 0.0001 & -0.0004 & -0.0010 & 0.0326 & -0.0516 & -0.0006 & -0.0020 & 0.6508 \end{bmatrix} \tag{69}$$

For the BIRE aircraft, aileron command depends primarily on yaw and roll rates. The stabilator command depends primarily on elevation angle, pitch rate, and yaw rate. The BIRE command depends primarily on yaw rate. Lastly, the throttle setting commands depends primarily on the elevation angle.

B. Closed-loop Properties

The closed-loop properties of the BIRE aircraft are determined from the system dynamics including the state-feedback matrix providing stability to the system.The eigenvalues of the BIRE closed-loop system matrix $(A - BK)$ calculated from the matrices presented in Eqs. (58), (59), and (69) are

$$\lambda_{cl} = \begin{bmatrix} -13.4586 + 0j \\ -5.8018 + 0j \\ -0.0995 + 0j \\ -0.5214 + 0.3568j \\ -0.5214 - 0.3568j \\ -1.0108 + 0j \\ -1.4351 + 0j \\ -1.2847 + 0j \\ -1.3391 + 0j \end{bmatrix} \tag{70}$$

which correspond to the eigenvectors

$$\chi_{cl} = \left\{ \begin{bmatrix} 0.0003 + 0j \\ -0.9446 + 0j \\ -0.0071 + 0j \\ 0.3271 + 0j \\ 0.0001 + 0j \\ -0.0075 + 0j \\ 0.0001 + 0j \\ -0.0243 + 0j \\ -0 + 0j \end{bmatrix}, \begin{bmatrix} 0.0435 + 0j \\ 0.0020 + 0j \\ -0.9989 + 0j \\ -0 + 0j \\ 0.0083 + 0j \\ 0 + 0j \\ 0.0161 + 0j \\ 0 + 0j \\ -0.0014 + 0j \end{bmatrix}, \begin{bmatrix} -0.9827 + 0j \\ -0 + 0j \\ 0.1428 + 0j \\ -0 + 0j \\ -0 + 0j \\ -0 + 0j \\ 0.1178 + 0j \\ 0 + 0j \\ 0.0003 + 0j \end{bmatrix}, \begin{bmatrix} 0.0360 - 0.0064j \\ -0.0002 - 0.0000j \\ -0.1549 + 0.3854j \\ 0 + 0j \\ -0.0003 + 0.0001j \\ -0 + 0j \\ 0.9089 + 0j \\ -0 - 0.0000j \\ 0.0005 + 0.0001j \end{bmatrix}, \begin{bmatrix} 0.0360 + 0.0064j \\ -0.0002 + 0j \\ -0.1549 - 0.3854j \\ 0 - 0.0000j \\ -0.0003 - 0.0001j \\ -0 - 0.0000j \\ 0.9089 - 0j \\ -0 + 0j \\ 0.0005 - 0.0001j \end{bmatrix}, \right.$$

$$\left. \begin{bmatrix} -0.0019 + 0j \\ 0.9981 + 0j \\ 0.0361 + 0j \\ -0.0274 + 0j \\ -0 + 0j \\ 0.0016 + 0j \\ -0.0305 + 0j \\ 0.0270 + 0j \\ 0 + 0j \end{bmatrix}, \begin{bmatrix} 0.0101 + 0j \\ -0.9644 + 0j \\ -0.2437 + 0j \\ -0.0043 + 0j \\ 0.0002 + 0j \\ -0.0022 + 0j \\ 0.1021 + 0j \\ 0.0031 + 0j \\ -0.0002 + 0j \end{bmatrix}, \begin{bmatrix} -0.0389 + 0j \\ 0.0011 + 0j \\ 0.8849 + 0j \\ -0 + 0j \\ -0.0006 + 0j \\ 0 + 0j \\ -0.4641 + 0j \\ 0 + 0j \\ 0.0005 + 0j \end{bmatrix}, \begin{bmatrix} 0.0292 + 0j \\ 0.6567 + 0j \\ -0.6787 + 0j \\ -0.0066 + 0j \\ 0.0005 + 0j \\ 0.0013 + 0j \\ 0.3273 + 0j \\ 0.0049 + 0j \\ -0.0004 + 0j \end{bmatrix} \right\} \quad (71)$$

Some inference can be made on the control design by comparing Tables 5 and the eigenvalues in Eq. (70). All eigenvalues for this system have been moved to the left half plane. The system is now stable. The solitary oscillatory mode is attributed to the phugoid mode. Though the BIRE closed-loop short period, Dutch roll, and rigid-body modes are stable, little more can be said regarding mode HQ. The spiral mode has become stable for the BIRE closed-loop system. The closed-loop short period mode for the BIRE is non-oscillatory. The BIRE, lacking a vertical tail, has a non-oscillatory closed-loop Dutch roll mode. In order to evaluate controller performance, the closed-loop system response is studied in time-domain and frequency-domain analyses as the modes in Eq. (70) are not traditional HQ modes.

V. Control Performance

While some dynamic modes for the closed-loop aircraft systems could be assigned HQ levels, the BIRE has closed-loop modes which cannot be characterized using traditional dynamic mode properties. Thus alternate techniques must be used to determine robustness of the BIRE aircraft control design. Analyses in the time and frequency domains can verify the robust properties of the control design.

A. Initial Condition Dispersion

First, response was simulated with initial condition dispersion for the BIRE with nonlinear dynamics and stabilizing state feedback. While the control design was performed on the Euler angle EOM formulation given in Eq. (40), the nonlinear simulations were performed using a quaternion dynamics formulation and a variable step integrator. For description and justification of the use of quaternions, the reader is directed to the work of Phillips where these themes are treated [54].

In simulation the aircraft was initialized at the trim condition. The rotation rates of the BIRE aircraft were then offset from the steady-level flight trim condition by each axis ($\Delta p = 90°$/s, $\Delta q = 10°$/s, $\Delta r = 2.5°$/s), and simulated for 15 seconds. The stabilizing controller response to this initial condition is shown in Fig. 2 for the BIRE aircraft. The blue lines in the control and control rate plots indicate the limits, as given in Table 3; on the control plot the black lines indicate the commanded control and the gray lines indicate the actuator state response.

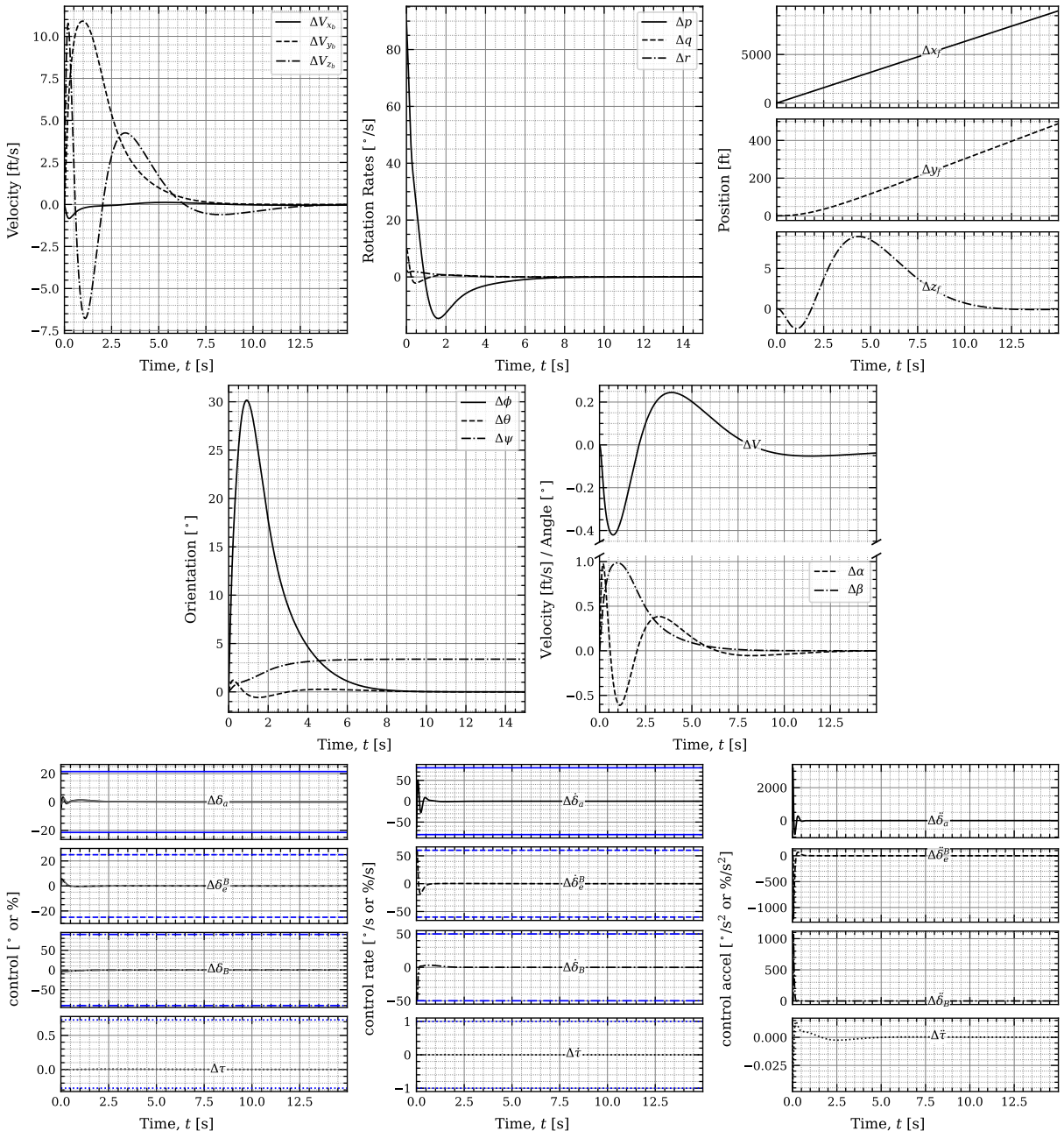

Fig. 2 BIRE response to initial condition dispersion.

Figure 2 shows the response of the BIRE aircraft to an initial condition dispersion. The states which are fed back return to zero within the 15 second simulation (excluding the body-fixed velocity V_{x_b}, which takes slightly longer). Those states which do not return to zero do not factor in the trim condition for the flat-Earth equations of motion (recall: x_f, y_f, ψ). This stabilization takes place within nearly 8 seconds, with the control near zero at 0.5 seconds. Though the controls are mostly actuated for only a short length of time, the aircraft takes longer to stabilize. Saturation of the control rates can be seen more clearly in Fig. 3.

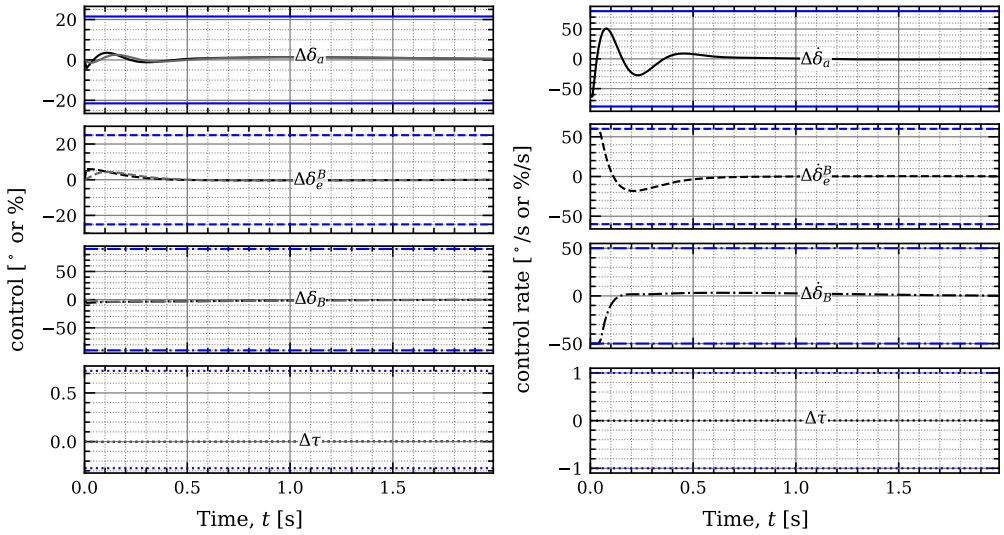

Fig. 3 BIRE control and control rate zoomed in response to initial condition dispersion.

The BIRE control response shown in Fig. 3 saturates in the rate limits on BIRE mechanism and stabilators. The BIRE throttle setting is not visibly actuated throughout the simulation. The BIRE controller achieves successful stabilization within the 15 second simulation.

B. Single Axis Angular Rate Dispersions and Region of Attraction

Monte Carlo simulations were run with normal random distributions of initial dispersions in p, q, and r. Each aircraft was simulated with single axis 1-sigma dispersions of $\sigma_{1\,p} = 120°/\text{s}$, $\sigma_{1\,q} = 40°/\text{s}$, and $\sigma_{1\,r} = 5°/\text{s}$. The results for these simulations are shown in Fig. 4. Each case is represented by a marker, with the color of the marker indicating the level of convergence. Shades from green toward yellow denote increasing time to convergence, with red denoting unconverged cases at the end of simulation (15 seconds). Convergence was determined as

$$\Delta y^T E \Delta y \leq 1 \tag{72}$$

where

$$E = \text{diag}\left(\begin{bmatrix} \Delta V_{x_b,\,\max} \\ \Delta V_{y_b,\,\max} \\ \Delta V_{z_b,\,\max} \\ \Delta p_{\max} \\ \Delta q_{\max} \\ \Delta r_{\max} \\ \Delta z_{f\,\max} \\ \Delta \phi_{\max} \\ \Delta \theta_{\max} \end{bmatrix}\right)^{-2} = \text{diag}\left(\begin{bmatrix} 10\ \text{ft/s} \\ 15\ \text{ft/s} \\ 15\ \text{ft/s} \\ 20°/\text{s} \\ 10°/\text{s} \\ 10°/\text{s} \\ 50\ \text{ft} \\ 25° \\ 10° \end{bmatrix}\right)^{-2} \tag{73}$$

The values in Eq. (73) were selected as 1-axis maximums for each state such that results for the Monte Carlo simulations with turbulence and error (presented in Fig. 6d) would have greater than or equal to 90% convergence success. Thus, greater attention should be paid to the convergence criterion than the convergence percentage successes.

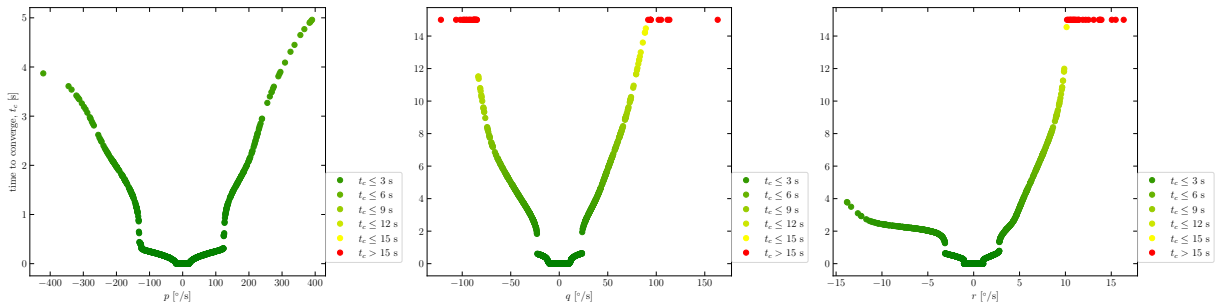

(a) Dispersions in p axis. **(b) Dispersions in q axis.** **(c) Dispersions in r axis.**

Fig. 4 BIRE single axis dispersions.

As shown in Fig. 4 the BIRE can stabilize with dispersions up to $\Delta p = \pm 360°/s$, $\Delta q = \pm 75°/s$, and $\Delta r = \pm 10°/s$. The BIRE is strongest in roll control and weakest in yaw control. A single ellipsoidal region of attraction was selected for continued analysis. This was selected so the success rate of the BIRE aircraft controller between sets of Monte Carlo simulations were comparable. This region is

$$\begin{aligned} \sigma_{1\,p} &= 100°/s \\ \sigma_{1\,q} &= 12°/s \\ \sigma_{1\,r} &= 3°/s \end{aligned} \tag{74}$$

Though such plots as in Fig. 4c appear to show severe limitations on the control design, the bounds given in Eq. (74) are large, and typical aircraft rate dispersions lie well within this region of attraction. Such large bounds are used in the present paper to demonstrate the limits of the presented control designs. The Monte Carlo initial condition dispersion simulation results and success rate for the BIRE are given in Fig. 6a.

C. Aerodynamic Model Error Dispersions

A similar single axis process was used to determine bounds on the acceptable aerodynamic forces and moments error. Monte Carlo simulations were run with the 1-sigma p, q, and r initial dispersions, as well as 1-sigma dispersions of $\epsilon_{C_A} = 0.25$ (1-sigma 25% normal random error in each force or moment coefficient C_A, applied as shown in Eq. (49)). The results for these simulations are shown in Fig. 5 for the BIRE, with convergence determined and marked as discussed for the single axis p, q, and r dispersions (see Eq. (72)).

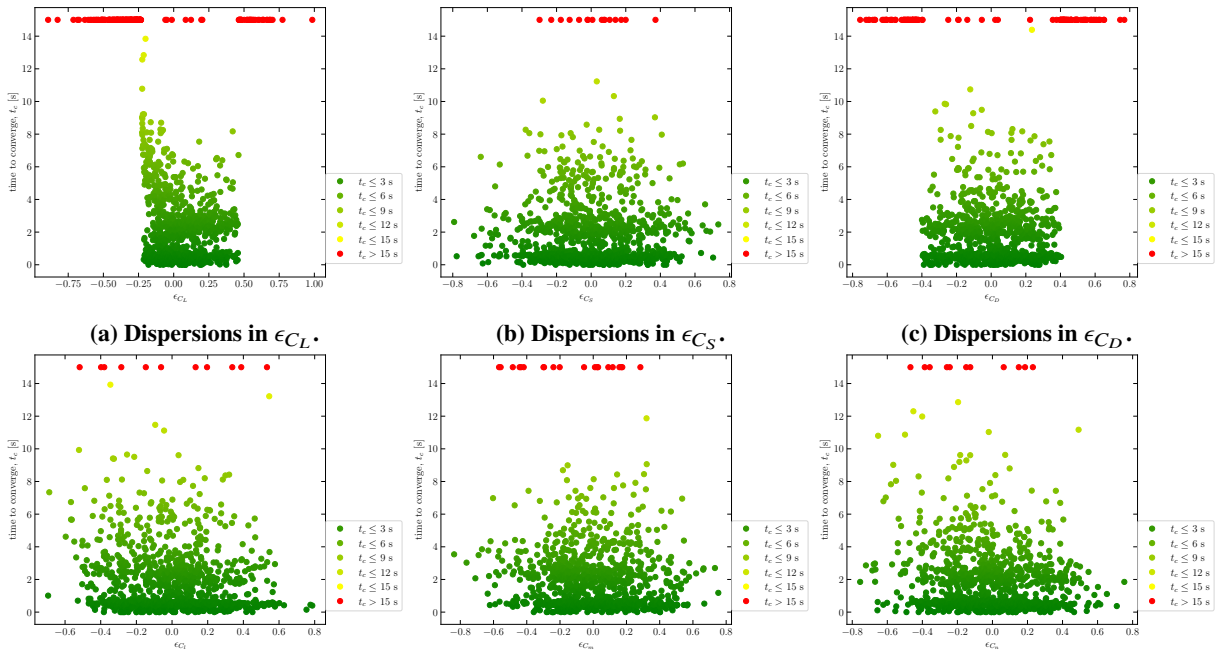

(a) Dispersions in ϵ_{C_L}. **(b) Dispersions in ϵ_{C_S}.** **(c) Dispersions in ϵ_{C_D}.**

(d) Dispersions in ϵ_{C_ℓ}. **(e) Dispersions in ϵ_{C_m}.** **(f) Dispersions in ϵ_{C_n}.**

Fig. 5 BIRE single force or moment error dispersions.

Based on Fig. 5, the aerodynamic error bounds for the BIRE aircraft to be used in further Monte Carlo analysis are prescribed to be

$$\begin{aligned} -0.24 < \epsilon_{C_L} &< 0.50 \\ \epsilon_{C_S} &= \pm 0.75 \\ \epsilon_{C_D} &= \pm 0.40 \\ \epsilon_{C_\ell} &= \pm 0.75 \\ \epsilon_{C_m} &= \pm 0.75 \\ \epsilon_{C_n} &= \pm 0.75 \end{aligned} \tag{75}$$

The 1-sigma values for the implemented force and moment errors are thus

$$\begin{aligned} \sigma_{1\,C_L} &= 0.07 \\ \sigma_{1\,C_S} &= 0.25 \\ \sigma_{1\,C_D} &= 0.12 \\ \sigma_{1\,C_\ell} &= 0.25 \\ \sigma_{1\,C_m} &= 0.25 \\ \sigma_{1\,C_n} &= 0.25 \end{aligned} \tag{76}$$

The BIRE aircraft is sensitive to error in lift coefficient. This is because the amount and direction of lift on the BIRE tail can significantly affect stability. Notably, though the BIRE is sensitive to yaw rate r dispersions, the BIRE is not sensitive to error in the aircraft yawing moment coefficient C_n. The BIRE is also sensitive to error in the drag coefficient C_D.

D. Monte Carlo Simulations with Perturbations

Aerodynamic model error and turbulence were applied to the Monte Carlo dispersions to determine the robust properties of the BIRE controller. Monte Carlo simulations are shown in Fig. 6. In each case the aircraft is initialized at trim with a random normal dispersion in p, q, and r, and simulated 1000 times for 15 seconds with and without random normal aerodynamic forces and moment error (as in Eq. (76)) and `light` turbulence. The convergence criterion was

the same as discussed for the single axis p, q, and r dispersions, given in Eq. (72). Note, the turbulence signal was pre-computed and linearly interpolated in between time steps to speed up case run time.

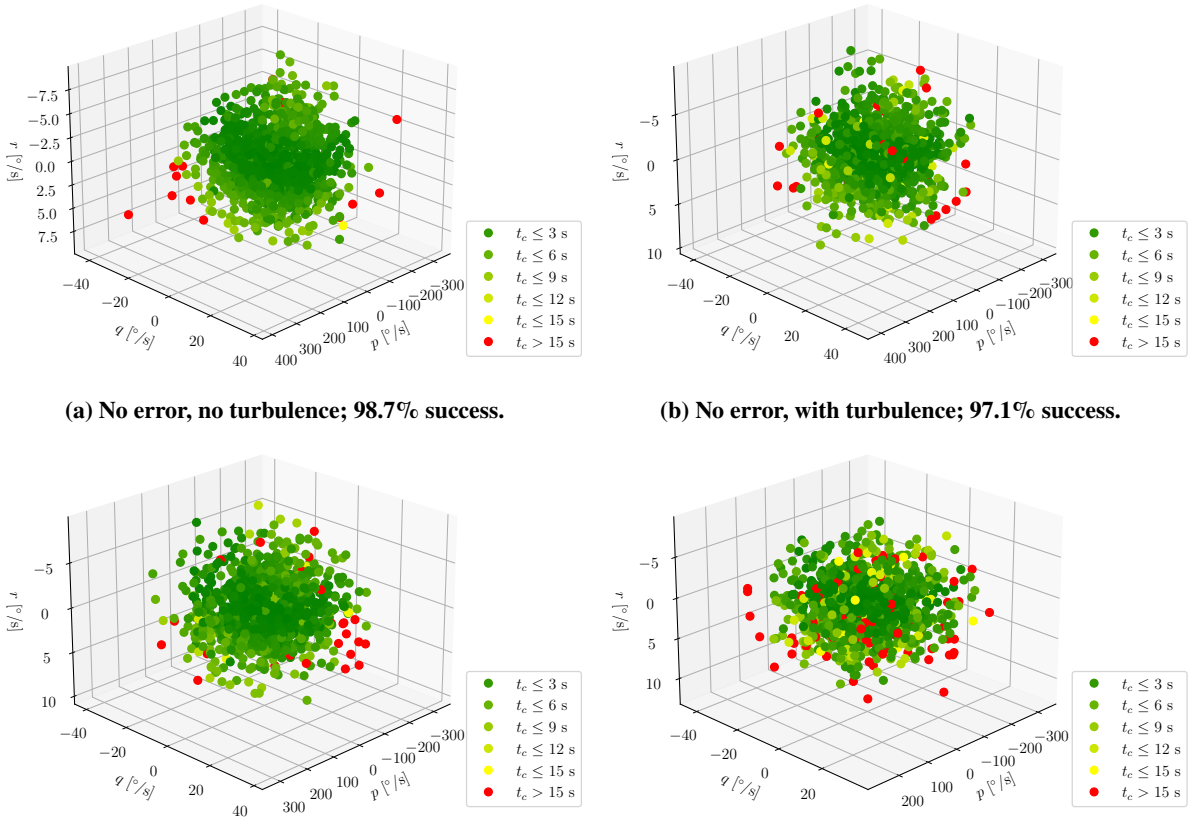

(a) No error, no turbulence; 98.7% success.

(b) No error, with turbulence; 97.1% success.

(c) With error, no turbulence; 97.1% success.

(d) With error, with turbulence; 91.1% success.

Fig. 6 BIRE simulations with various disturbance types.

Figure 6 shows the effect of turbulence and model error on the BIRE aircraft. The majority of the simulations converge within 3 seconds, with some in each case converging between 3 and 15 seconds. `Light` turbulence caused a 1.6% decrease in controller success, with error also causing a 1.6% decrease in success. The additive case of error and turbulence had a greater effect (7.6%). The BIRE cases which take greater time to converge tend to occur on the largest combined dispersions in the yaw rate and pitch rate of the same sign (i.e. +p+r and -p-r). With such large initial condition dispersions, these results are acceptable for the BIRE aircraft controller. The unconverged cases generally lie on or near the border of the region of attraction.

E. Frequency Domain

A key aspect of the control design are the controller properties in the frequency domain. One fundamental metric of the control design are the input singular values. For multiple-input multiple output systems, desireable singular values are (for the minimum singular value) large at low frequencies and (for the maximum singular value) small at high frequencies [7]. The input singular values for the BIRE aircraft are shown in Fig. 7.

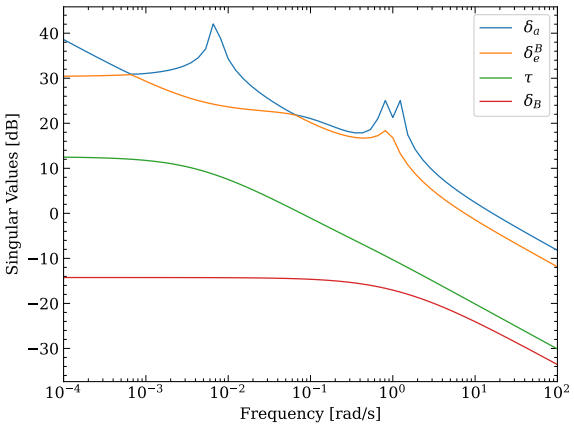

Fig. 7 BIRE controller input singular values.

The singular value curves for the throttle and BIRE actuator are poorly shaped. Inspection of time-domain results suggests these actuators are little used, and these facts motivate the following question: how does the BIRE aircraft perform if BIRE and throttle setting are excluded from the control design?

F. Controller Performance Excluding δ_B, τ

Neglecting inputs for a control design involves removing columns from the control matrix B and columns and rows from the input weightings matrix R. Note that the system remains controllable with these two columns removed. The closed-loop system eigenvalues for the BIRE control design neglecting δ_B, τ, and δ_B and τ are

$$\lambda_{cl_{\not\delta_B}} = \begin{bmatrix} -13.4586 + 0j \\ -5.8018 + 0j \\ -0.0995 + 0j \\ -0.5214 + 0.3568j \\ -0.5214 - 0.3568j \\ -1.0108 + 0j \\ -1.4346 + 0j \\ -1.2847 + 0j \\ -1.3396 + 0j \end{bmatrix}, \quad \lambda_{cl_{\not\tau}} = \begin{bmatrix} -13.4586 + 0j \\ -5.8018 + 0j \\ -0.0031 + 0j \\ -0.5218 + 0.3564j \\ -0.5218 - 0.3564j \\ -1.0108 + 0j \\ -1.4351 + 0j \\ -1.2847 + 0j \\ -1.3391 + 0j \end{bmatrix}, \quad \lambda_{cl_{\not\delta_B,\not\tau}} = \begin{bmatrix} -13.4586 + 0j \\ -5.8018 + 0j \\ -0.0031 + 0j \\ -0.5218 + 0.3564j \\ -0.5218 - 0.3564j \\ -1.0108 + 0j \\ -1.4346 + 0j \\ -1.2847 + 0j \\ -1.3396 + 0j \end{bmatrix} \tag{77}$$

The closed-loop dynamics are minimally effected by neglecting either or both of the BIRE and throttle inputs. Comparing to the full input closed-loop eigenvalues in Eq. (70) shows the effect of neglecting control effectors from the control design. Neglecting the BIRE mechanism has minor effect on certain modes and neglecting the throttle setting has minor effects on other modes. Notably neglecting the BIRE most only affects lateral handling qualities and neglecting the throttle most only affect longitudinal handling qualities.

Convergence success rates for each type of control design are presented in Table 6. Each case with error is run with the same error 1-sigma values shown in Eq. (76), and each case with turbulence is run on a `light` setting, with all cases having initial condition dispersions as in Eq. (74).

Error	Turbulence	δ_B, τ	$\cancel{\delta_B}, \tau$	$\delta_B, \cancel{\tau}$	$\cancel{\delta_B}, \cancel{\tau}$
		98.7%	97.5%	98.4%	96.9%
	✓	97.1%	96.5%	97.1%	93.7%
✓		97.1%	96.4%	87.7%	86.8%
✓	✓	91.1%	91.7%	79.5%	76.7%

Table 6 Monte Carlo simulations convergence success for controllers excluding δ_B, τ.

Neglecting only the BIRE actuator results in at most a 1.2% decrease in success, and neglecting only the throttle command results in a decrease of at most 11.6%. Excluding both control effectors results in at most a 14.6% decrease in convergence success. This suggests the BIRE and throttle could be neglected from the control design with minor consequence. A final justification for this decision is given in Fig. 8.

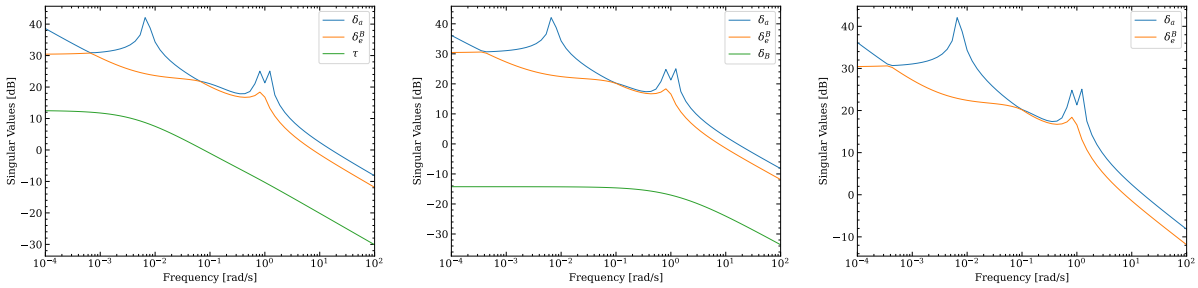

(a) $\cancel{\delta_B}$ **(b)** $\cancel{\tau}$ **(c)** $\cancel{\delta_B}, \cancel{\tau}$

Fig. 8 BIRE controller excluding δ_B, τ input singular values.

Neglecting both the BIRE mechanism and throttle setting from the control design results in acceptable controller performance input properties. As shown in Fig. 8 it would be preferable to neglect the BIRE actuator from the control design. Though the throttle input singular values in Fig. 8a are more desirable than those for the BIRE in Fig. 8b, these results show the throttle setting may be better incorporated in a different control design. Similarly, the convergence successes in Table 6 suggest the BIRE actuator can be dropped with no consequence, and throttle should be removed from the stabilizing control law and included as input to a different control loop (i.e. a speed controller). Whether the BIRE control design includes or excludes the BIRE and throttle inputs, each controller is robust in time-domain analyses, with greater success when only neglecting the BIRE actuator.

VI. Conclusion

A stabilizing controller was built for the bio-inspired variant of a statically-unstable baseline fighter aircraft. Because actuator capabilities form a crucial component of control performance, the present paper outlined the control design for the BIRE aircraft with first-order actuator dynamics, deflection limits, and rate limits. The EOM Euler angle formulation was presented. First-order actuator dynamics were then incorporated into the aircraft dynamics. The linearized EOM were given and the linearized system was calculated for each aircraft trimmed in steady level flight at the Air Combat Maneuver Condition.

Analyses were performed to evaluate the BIRE controller, with the aircraft Earth-fixed x- and y-positions and heading angle ψ states removed from the state feedback control design. An LQR controller was designed and presented for the BIRE aircraft. Weightings were chosen for quality performance as determined in time-domain and frequency-domain analyses. While the BIRE aircraft has instabilities in the uncontrolled system, the closed-loop system has stable eigenvalues with acceptable response characteristics.

Time-domain performance of the controller was assessed based on Monte Carlo simulations with initial condition dispersions, atmospheric turbulence, and aerodynamic force and moment errors. Frequency-domain performance was assessed based on input singular values. The BIRE mechanism and throttle setting are not used significantly in

simulation of the BIRE aircraft. As shown in time-domain and frequency-domain analyses, the BIRE control input can be neglected from the control design with minimal effect.

Further control development for this bio-inspired fighter is recommended, particularly using nonlinear techniques which may be more suited for the BIRE system. In further control development it may be more appropriate to feedback total velocity and aerodynamic angles rather than the body-fixed aircraft velocities. Further work should examine controller performance at multiple trim conditions by varying altitude, airspeed, as well as steady-coordinated turns. In such analyses it would be prudent to examine whether the BIRE and throttle inputs can also be neglected in control design at these conditions. Further work should study implementation of a tracking control design for the BIRE aircraft.

A. Aircraft Properties

A. Aircraft Geometric and Mass Properties

Table A.1 Baseline and BIRE shared geometric and angular momentum characteristics.

Property	Value
S_w [ft]	300
b_w [ft]	30
$\bar{c}_w$ [ft]	11.32
h_{x_b} [slugs-ft^2/sec]	160
h_{y_b} [slugs-ft^2/sec]	0
h_{z_b} [slugs-ft^2/sec]	0

Table A.2 Baseline weight and inertia characteristics.

W [lbf]	20500
I_{xx_b} [slugs-ft^2]	9496
I_{yy_b} [slugs-ft^2]	55814
I_{zz_b} [slugs-ft^2]	63100
I_{xy_b} [slugs-ft^2]	0
I_{xz_b} [slugs-ft^2]	982
I_{yz_b} [slugs-ft^2]	0

Table A.3 BIRE weight and inertia characteristics.

W [lbf]	21000			
	A [slugs-ft^2]	ω	ϕ	z [slugs-ft^2]
I_{xx_b}	0	0	0	9280
I_{yy_b}	-160.8070	2	1.5708	58287.8610
I_{zz_b}	160.8350	2	1.5708	65605.6027
I_{xy_b}	0	0	0	0
I_{xz_b}	0	0	0	-5
I_{yz_b}	-160.5850	2	0	160.5850

B. Aircraft Aerodynamic Model Coefficients

Table A.4 Baseline aerodynamic model force coefficients.

Coefficient	Value
C_{L_0}	0.0456
$C_{L,\alpha}$	3.5791
$C_{L,\bar{q}}$	3.3916
C_{L,δ_e}	0.5652
$C_{S,\beta}$	-0.9009
$C_{S,\bar{p}}$	-0.0153
$C_{S,L\bar{p}}$	0.3318
$C_{S,\bar{r}}$	0.4357
C_{S,δ_a}	0.0656
C_{S,δ_r}	0.1698
C_{D_0}	0.0218
$C_{D,L}$	-0.0340
C_{D,L^2}	0.1834
C_{D,S^2}	0.6081
$C_{D,S\bar{p}}$	0.0768
$C_{D,\bar{q}}$	0.0368
$C_{D,L\bar{q}}$	0.7750
$C_{D,L^2\bar{q}}$	-0.1844
$C_{D,S\bar{r}}$	-0.7239
C_{D,δ_e}	-0.0032
$C_{D,L\delta_e}$	0.1775
C_{D,δ_e^2}	0.2854
$C_{D,S\delta_a}$	0.1118
$C_{D,S\delta_r}$	0.1604

Table A.5 Baseline aerodynamic model moment coefficients.

Coefficient	Value
$C_{\ell,\beta}$	-0.0786
$C_{\ell,\bar{p}}$	-0.3182
$C_{\ell,\bar{r}}$	0.0469
$C_{\ell,L\bar{r}}$	0.1067
C_{ℓ,δ_a}	-0.0741
C_{ℓ,δ_r}	0.0257
C_{m_0}	-0.0097
$C_{m,\alpha}$	0.1766
$C_{m,\bar{q}}$	-4.8503
C_{m,δ_e}	-0.5881
$C_{n,\beta}$	0.2426
$C_{n,\bar{p}}$	0.0131
$C_{n,L\bar{p}}$	-0.1005
$C_{n,\bar{r}}$	-0.1787
C_{n,δ_a}	-0.0276
$C_{n,L\delta_a}$	0.0077
C_{n,δ_r}	-0.0899

Table A.6 BIRE aerodynamic model force coefficients.

Coefficient	A	ω	ϕ	z
$\hat{C}_{L_0}$	-0.0144	2	1.5708	0.0621
$\hat{C}_{L,\alpha}$	0.1091	2	1.5708	3.5469
$\hat{C}_{L,\beta}$	-0.7216	2	0	0
$\hat{C}_{L,\bar{p}}$	0	0	0	0
$\hat{C}_{L,\bar{q}}$	2.0262	2	1.5708	1.5469
$\hat{C}_{L,\bar{r}}$	0.6798	2	0	0
$\hat{C}_{L,\delta_a}$	0	0	0	-0.0007
$\hat{C}_{L,\delta_e^B}$	0.7646	1	1.5708	-0.1822
$\hat{C}_{S_0}$	-0.0106	2	0	0
$\hat{C}_{S,\alpha}$	0.1834	2	0	0
$\hat{C}_{S,\beta}$	0.6805	2	1.5708	-0.8493
$\hat{C}_{S,\bar{p}}$	0	0	0	-0.0022
$\hat{C}_{S,L\bar{p}}$	0.0192	2	1.5708	0.2233
$\hat{C}_{S,\bar{q}}$	1.9916	2	0	0
$\hat{C}_{S,\bar{r}}$	-0.6134	2	1.5708	0.5976
$\hat{C}_{S,\delta_a}$	0.0015	2	1.5708	-0.0524
$\hat{C}_{S,\delta_e^B}$	0.7352	1	0	0
$\hat{C}_{D_0}$	0	0	0	0.0209
$\hat{C}_{D,L}$	0	0	0	-0.0332
$\hat{C}_{D,L^2}$	0.0047	4	1.5708	0.1767
$\hat{C}_{D,S}$	0.0255	2	0	-0.0000
$\hat{C}_{D,S^2}$	0.3082	2	1.5708	0.6364
$\hat{C}_{D,\bar{p}}$	0	0	0	0
$\hat{C}_{D,S\bar{p}}$	0	0	0	0.0013
$\hat{C}_{D,\bar{q}}$	0	0	0	0.0261
$\hat{C}_{D,L\bar{q}}$	0.3883	2	1.5708	0.3700
$\hat{C}_{D,L^2\bar{q}}$	0	0	0	-0.0303
$\hat{C}_{D,\bar{r}}$	0	0	0	0
$\hat{C}_{D,S\bar{r}}$	0	0	0	-0.1146
$\hat{C}_{D,\delta_a}$	-0.0079	2	0	0.0000
$\hat{C}_{D,S\delta_a}$	0.0492	2	1.5708	-0.0381
$\hat{C}_{D,\delta_e^B}$	-0.0061	1	1.5708	0.0015
$\hat{C}_{D,L\delta_e^B}$	0.1830	1	1.5708	0
$\hat{C}_{D,\delta_e^{B\,2}}$	-0.0950	1	1.5708	0.4244

Table A.7 BIRE aerodynamic model moment coefficients.

Coefficient	A	ω	ϕ	z
$\hat{C}_{\ell_0}$	0.0002	2	0	0
$\hat{C}_{\ell,\alpha}$	-0.0023	4	0	0
$\hat{C}_{\ell,\beta}$	0.0017	2	1.5708	-0.0283
$\hat{C}_{\ell,\bar{p}}$	0.0040	2	1.5708	-0.3069
$\hat{C}_{\ell,\bar{q}}$	0	0	0	0
$\hat{C}_{\ell,\bar{r}}$	0	0	0	0.0062
$\hat{C}_{\ell,L\bar{r}}$	0	0	0	0.1104
$\hat{C}_{\ell,\delta_a}$	0.0140	2	1.5708	-0.1065
$\hat{C}_{\ell,\delta_e^B}$	0.0017	1	0	0
$\hat{C}_{m_0}$	0.0164	2	1.5708	-0.0218
$\hat{C}_{m,\alpha}$	-0.1381	2	1.5708	0.2720
$\hat{C}_{m,\beta}$	0.8299	2	0	0
$\hat{C}_{m,\bar{p}}$	-0.0102	2	0	0
$\hat{C}_{m,\bar{q}}$	-2.3551	2	1.5708	-2.5457
$\hat{C}_{m,\bar{r}}$	-0.7667	2	0	0
$\hat{C}_{m,\delta_a}$	0.0008	2	0	-0.0007
$\hat{C}_{m,\delta_e^B}$	-0.9115	1	1.5708	0.2914
$\hat{C}_{n_0}$	0.0048	2	0	0
$\hat{C}_{n,\alpha}$	-0.0929	2	0	0
$\hat{C}_{n,\beta}$	-0.3176	2	1.5708	0.2804
$\hat{C}_{n,\bar{p}}$	0	0	0	0.0010
$\hat{C}_{n,L\bar{p}}$	-0.0074	2	1.5708	-0.0621
$\hat{C}_{n,\bar{q}}$	-0.9205	2	0	0
$\hat{C}_{n,\bar{r}}$	0.2894	2	1.5708	-0.2789
$\hat{C}_{n,\delta_a}$	0	0	0	0.0131
$\hat{C}_{n,L\delta_a}$	-0.0169	2	1.5708	0.0411
$\hat{C}_{n,\delta_e^B}$	-0.3527	1	0	0

B. Dynamics Linearization

Here is given the linearization for the system given in Eq. (50). As with the system description in Section II, the linearization will be developed first from state and control derivatives of the incompressible aerodynamic model. These will then be incorporated into the compressibility correction derivatives. With the propulsive derivatives, the aerodynamic derivatives will then be included in the derivatives of the dimensional body-fixed forces and moments with respect to aircraft state and input. A final formulated A and B matrix are then presented. Though this linearization is performed with respect to the control input u, the subscript $_{cmd}$ is excluded from the nomenclature for brevity.

For convenience in the linearization process, note the following partial derivatives of the aerodynamic angles and dimensionless rotation rates with respect to body-fixed velocity:

$$\alpha_{,V_{x_b}} = -\frac{V_{z_b}}{V_{x_b}^2 + V_{z_b}^2}, \quad \alpha_{,V_{z_b}} = \frac{V_{x_b}}{V_{x_b}^2 + V_{z_b}^2} \tag{B.1}$$

$$\beta_{,V_{x_b}} = -\frac{V_{x_b} V_{y_b}}{V^2 \sqrt{V_{x_b}^2 + V_{z_b}^2}}, \quad \beta_{,V_{y_b}} = \frac{\sqrt{V_{x_b}^2 + V_{z_b}^2}}{V^2}, \quad \beta_{,V_{z_b}} = -\frac{V_{y_b} V_{z_b}}{V^2 \sqrt{V_{x_b}^2 + V_{z_b}^2}} \tag{B.2}$$

$$\bar{p}_{,V_{x_b}} = -\bar{p}\frac{V_{x_b}}{V^2}, \quad \bar{p}_{,V_{y_b}} = -\bar{p}\frac{V_{y_b}}{V^2}, \quad \bar{p}_{,V_{z_b}} = -\bar{p}\frac{V_{z_b}}{V^2} \tag{B.3}$$

$$\bar{q}_{,V_{x_b}} = -\bar{q}\frac{V_{x_b}}{V^2}, \quad \bar{q}_{,V_{y_b}} = -\bar{q}\frac{V_{y_b}}{V^2}, \quad \bar{q}_{,V_{z_b}} = -\bar{q}\frac{V_{z_b}}{V^2} \tag{B.4}$$

$$\bar{r}_{,V_{x_b}} = -\bar{r}\frac{V_{x_b}}{V^2}, \quad \bar{r}_{,V_{y_b}} = -\bar{r}\frac{V_{y_b}}{V^2}, \quad \bar{r}_{,V_{z_b}} = -\bar{r}\frac{V_{z_b}}{V^2} \tag{B.5}$$

A. Baseline Aerodynamic Force and Moment Derivatives with respect to State

The aerodynamic force and moment derivatives with respect to state will first be determined for the baseline aircraft. The derivatives of lift coefficient with respect to state are

$$\mathring{C}_{L,V_{x_b}} = C_{L,\alpha}\alpha_{,V_{x_b}} + C_{L,\bar{q}}\bar{q}_{,V_{x_b}} \tag{B.6}$$

$$\mathring{C}_{L,V_{y_b}} = C_{L,\bar{q}}\bar{q}_{,V_{y_b}} \tag{B.7}$$

$$\mathring{C}_{L,V_{z_b}} = C_{L,\alpha}\alpha_{,V_{z_b}} + C_{L,\bar{q}}\bar{q}_{,V_{z_b}} \tag{B.8}$$

$$\mathring{C}_{L,q} = C_{L,\bar{q}}R_{lon} \tag{B.9}$$

The derivatives of side-force coefficient with respect to state are

$$\mathring{C}_{S,V_{x_b}} = C_{S,\beta}\beta_{,V_{x_b}} + C_{S,L\bar{p}}C_{L,\alpha}\alpha_{,V_{x_b}}\bar{p} + (C_{S,L\bar{p}}C_{L_1} + C_{S,\bar{p}})\bar{p}_{,V_{x_b}} + C_{S,\bar{r}}\bar{r}_{,V_{x_b}} \tag{B.10}$$

$$\mathring{C}_{S,V_{y_b}} = C_{S,\beta}\beta_{,V_{y_b}} + (C_{S,L\bar{p}}C_{L_1} + C_{S,\bar{p}})\bar{p}_{,V_{y_b}} + C_{S,\bar{r}}\bar{r}_{,V_{y_b}} \tag{B.11}$$

$$\mathring{C}_{S,V_{z_b}} = C_{S,\beta}\beta_{,V_{z_b}} + C_{S,L\bar{p}}C_{L,\alpha}\alpha_{,V_{z_b}}\bar{p} + (C_{S,L\bar{p}}C_{L_1} + C_{S,\bar{p}})\bar{p}_{,V_{z_b}} + C_{S,\bar{r}}\bar{r}_{,V_{z_b}} \tag{B.12}$$

$$\mathring{C}_{S,p} = (C_{S,L\bar{p}}C_{L_1} + C_{S,\bar{p}})R_{lat} \tag{B.13}$$

$$\mathring{C}_{S,r} = C_{S,\bar{r}}R_{lat} \tag{B.14}$$

The derivatives of drag coefficient with respect to state are

$$\begin{aligned}\mathring{C}_{D,V_{x_b}} = {} & \left(C_{D,L} + 2C_{D,L^2}C_{L_1} + \left(2C_{D,L^2\bar{q}}C_{L_1} + C_{D,L\bar{q}}\right)\bar{q} + C_{D,L\delta_e}\delta_e\right)C_{L,\alpha}\alpha_{,V_{x_b}} \\ & + \left(2C_{D,S^2}C_{S_1} + C_{D,S\bar{p}}\bar{p} + C_{D,S\bar{r}}\bar{r} + C_{D,S\delta_a}\delta_a + C_{D,S\delta_r}\delta_r\right)C_{S,\beta}\beta_{,V_{x_b}} \\ & + C_{D,S\bar{p}}C_{S_1}\bar{p}_{,V_{x_b}} + \left(C_{D,L^2\bar{q}}C_{L_1}^2 + C_{D,L\bar{q}}C_{L_1} + C_{D,\bar{q}}\right)\bar{q}_{,V_{x_b}} + C_{D,S\bar{r}}C_{S_1}\bar{r}_{,V_{x_b}}\end{aligned} \tag{B.15}$$

$$\begin{aligned}\mathring{C}_{D,V_{y_b}} = {} & \left(2C_{D,S^2}C_{S_1} + C_{D,S\bar{p}}\bar{p} + C_{D,S\bar{r}}\bar{r} + C_{D,S\delta_a}\delta_a + C_{D,S\delta_r}\delta_r\right)C_{S,\beta}\beta_{,V_{y_b}} \\ & + C_{D,S\bar{p}}C_{S_1}\bar{p}_{,V_{y_b}} + \left(C_{D,L^2\bar{q}}C_{L_1}^2 + C_{D,L\bar{q}}C_{L_1} + C_{D,\bar{q}}\right)\bar{q}_{,V_{y_b}} + C_{D,S\bar{r}}C_{S_1}\bar{r}_{,V_{y_b}}\end{aligned} \tag{B.16}$$

$$\begin{aligned}\mathring{C}_{D,V_{z_b}} = {} & \left(C_{D,L} + 2C_{D,L^2}C_{L_1} + \left(2C_{D,L^2\bar{q}}C_{L_1} + C_{D,L\bar{q}}\right)\bar{q} + C_{D,L\delta_e}\delta_e\right)C_{L,\alpha}\alpha_{,V_{z_b}} \\ & + \left(2C_{D,S^2}C_{S_1} + C_{D,S\bar{p}}\bar{p} + C_{D,S\bar{r}}\bar{r} + C_{D,S\delta_a}\delta_a + C_{D,S\delta_r}\delta_r\right)C_{S,\beta}\beta_{,V_{z_b}} \\ & + C_{D,S\bar{p}}C_{S_1}\bar{p}_{,V_{z_b}} + \left(C_{D,L^2\bar{q}}C_{L_1}^2 + C_{D,L\bar{q}}C_{L_1} + C_{D,\bar{q}}\right)\bar{q}_{,V_{z_b}} + C_{D,S\bar{r}}C_{S_1}\bar{r}_{,V_{z_b}}\end{aligned} \tag{B.17}$$

$$\mathring{C}_{D,p} = C_{D,S\bar{p}}C_{S_1}R_{lat} \tag{B.18}$$

$$\mathring{C}_{D,q} = \left(C_{D,L^2\bar{q}}C_{L_1}^2 + C_{D,L\bar{q}}C_{L_1} + C_{D,\bar{q}}\right)R_{lon} \tag{B.19}$$

$$\mathring{C}_{D,r} = C_{D,S\bar{r}}C_{S_1}R_{lat} \tag{B.20}$$

The derivatives of rolling moment coefficient with respect to state are

$$\mathring{C}_{\ell,V_{x_b}} = C_{\ell,\beta}\beta_{,V_{x_b}} + C_{\ell,\bar{p}}\bar{p}_{,V_{x_b}} + C_{\ell,L\bar{r}}C_{L,\alpha}\alpha_{,V_{x_b}}\bar{r} + (C_{\ell,L\bar{r}}C_{L_1} + C_{\ell,\bar{r}})\bar{r}_{,V_{x_b}} \tag{B.21}$$

$$\mathring{C}_{\ell,V_{y_b}} = C_{\ell,\beta}\beta_{,V_{y_b}} + C_{\ell,\bar{p}}\bar{p}_{,V_{y_b}} + (C_{\ell,L\bar{r}}C_{L_1} + C_{\ell,\bar{r}})\bar{r}_{,V_{y_b}} \tag{B.22}$$

$$\mathring{C}_{\ell,V_{z_b}} = C_{\ell,\beta}\beta_{,V_{z_b}} + C_{\ell,\bar{p}}\bar{p}_{,V_{z_b}} + C_{\ell,L\bar{r}}C_{L,\alpha}\alpha_{,V_{z_b}}\bar{r} + (C_{\ell,L\bar{r}}C_{L_1} + C_{\ell,\bar{r}})\bar{r}_{,V_{z_b}} \tag{B.23}$$

$$\mathring{C}_{\ell,p} = C_{\ell,\bar{p}}R_{lat} \tag{B.24}$$

$$\mathring{C}_{\ell,r} = (C_{\ell,L\bar{r}} C_{L_1} + C_{\ell,\bar{r}}) R_{lat} \tag{B.25}$$

The derivatives of pitching moment coefficient with respect to state are

$$\mathring{C}_{m,V_{x_b}} = C_{m,\alpha}\alpha_{,V_{x_b}} + C_{m,\bar{q}}\bar{q}_{,V_{x_b}} \tag{B.26}$$

$$\mathring{C}_{m,V_{y_b}} = C_{m,\bar{q}}\bar{q}_{,V_{y_b}} \tag{B.27}$$

$$\mathring{C}_{m,V_{z_b}} = C_{m,\alpha}\alpha_{,V_{z_b}} + C_{m,\bar{q}}\bar{q}_{,V_{z_b}} \tag{B.28}$$

$$\mathring{C}_{m,q} = C_{m,\bar{q}} R_{lon} \tag{B.29}$$

The derivatives of yawing moment coefficient with respect to state are

$$\mathring{C}_{n,V_{x_b}} = \left(C_{n,L\bar{p}}\bar{p} + C_{n,L\delta_a}\delta_a\right) C_{L,\alpha}\alpha_{,V_{x_b}} + C_{n,\beta}\beta_{,V_{x_b}} + (C_{n,L\bar{p}} C_{L_1} + C_{n,\bar{p}})\bar{p}_{,V_{x_b}} + C_{n,\bar{r}}\bar{r}_{,V_{x_b}} \tag{B.30}$$

$$\mathring{C}_{n,V_{y_b}} = C_{n,\beta}\beta_{,V_{y_b}} + (C_{n,L\bar{p}} C_{L_1} + C_{n,\bar{p}})\bar{p}_{,V_{y_b}} + C_{n,\bar{r}}\bar{r}_{,V_{y_b}} \tag{B.31}$$

$$\mathring{C}_{n,V_{z_b}} = \left(C_{n,L\bar{p}}\bar{p} + C_{n,L\delta_a}\delta_a\right) C_{L,\alpha}\alpha_{,V_{z_b}} + C_{n,\beta}\beta_{,V_{z_b}} + (C_{n,L\bar{p}} C_{L_1} + C_{n,\bar{p}})\bar{p}_{,V_{z_b}} + C_{n,\bar{r}}\bar{r}_{,V_{z_b}} \tag{B.32}$$

$$\mathring{C}_{n,p} = (C_{n,L\bar{p}} C_{L_1} + C_{n,\bar{p}}) R_{lat} \tag{B.33}$$

$$\mathring{C}_{n,r} = C_{n,\bar{r}} R_{lat} \tag{B.34}$$

where

$$R_{lon} = \frac{\bar{c}_w}{2V} \tag{B.35}$$

$$R_{lat} = \frac{b_w}{2V} \tag{B.36}$$

Note the following negligible derivatives for the baseline

$$\mathring{C}_{L,p} = \mathring{C}_{L,r} = \mathring{C}_{S,q} = \mathring{C}_{\ell,q} = \mathring{C}_{m,p} = \mathring{C}_{m,r} = \mathring{C}_{n,q} = 0 \tag{B.37}$$

B. Baseline Aerodynamic Force and Moment Derivatives with respect to Input

Next, the aerodynamic force and moment derivatives with respect to input for the baseline aircraft will be determined. The derivatives of drag coefficient with respect to input are

$$\mathring{C}_{D,\delta_a} = C_{D,S\delta_a} C_{S_1} \tag{B.38}$$

$$\mathring{C}_{D,\delta_e} = C_{D,L\delta_e} C_{L_1} + C_{D,\delta_e} + 2C_{D,\delta_e^2}\delta_e \tag{B.39}$$

$$\mathring{C}_{D,\delta_r} = C_{D,S\delta_r} C_{S_1} \tag{B.40}$$

The derivatives of yawing moment coefficient with respect to input are

$$\mathring{C}_{n,\delta_a} = C_{n,L\delta_a} C_{L_1} + C_{n,\delta_a} \tag{B.41}$$

The following coefficients are equivalent to those shown in the aerodynamic model given in Eqs. (8) – (15) (i.e. $\mathring{C}_{L,\delta_e} = C_{L,\delta_e}$)

$$\mathring{C}_{L,\delta_e}, \mathring{C}_{S,\delta_a}, \mathring{C}_{S,\delta_r}, \mathring{C}_{\ell,\delta_a}, \mathring{C}_{\ell,\delta_r}, \mathring{C}_{m,\delta_e}, \mathring{C}_{n,\delta_r} \tag{B.42}$$

Note the following negligible derivatives for the baseline

$$\mathring{C}_{L,\delta_a} = \mathring{C}_{L,\delta_r} = \mathring{C}_{S,\delta_e} = \mathring{C}_{\ell,\delta_e} = \mathring{C}_{m,\delta_a} = \mathring{C}_{m,\delta_r} = \mathring{C}_{n,\delta_e} = 0 \tag{B.43}$$

C. BIRE Aerodynamic Force and Moment Derivatives with respect to State

The aerodynamic force and moment derivatives with respect to state will now be found for the BIRE. The derivatives of lift coefficient with respect to state are

$$\mathring{C}_{L,V_{x_b}} = \hat{C}_{L,\alpha}\alpha_{,V_{x_b}} + \hat{C}_{L,\beta}\beta_{,V_{x_b}} + \hat{C}_{L,\bar{p}}\bar{p}_{,V_{x_b}} + \hat{C}_{L,\bar{q}}\bar{q}_{,V_{x_b}} + \hat{C}_{L,\bar{r}}\bar{r}_{,V_{x_b}} \tag{B.44}$$

$$\mathring{C}_{L,V_{y_b}} = \hat{C}_{L,\beta}\beta_{,V_{y_b}} + \hat{C}_{L,\bar{p}}\bar{p}_{,V_{y_b}} + \hat{C}_{L,\bar{q}}\bar{q}_{,V_{y_b}} + \hat{C}_{L,\bar{r}}\bar{r}_{,V_{y_b}} \tag{B.45}$$

$$\mathring{C}_{L,V_{z_b}} = \hat{C}_{L,\alpha}\alpha_{,V_{z_b}} + \hat{C}_{L,\beta}\beta_{,V_{z_b}} + \hat{C}_{L,\bar{p}}\bar{p}_{,V_{z_b}} + \hat{C}_{L,\bar{q}}\bar{q}_{,V_{z_b}} + \hat{C}_{L,\bar{r}}\bar{r}_{,V_{z_b}} \tag{B.46}$$

$$\mathring{C}_{L,p} = \hat{C}_{L,\bar{p}}R_{lat} \tag{B.47}$$

$$\mathring{C}_{L,q} = \hat{C}_{L,\bar{q}}R_{lon} \tag{B.48}$$

$$\mathring{C}_{L,r} = \hat{C}_{L,\bar{r}}R_{lat} \tag{B.49}$$

The derivatives of side-force coefficient with respect to state are

$$\mathring{C}_{S,V_{x_b}} = \hat{C}_{S,\alpha}\alpha_{,V_{x_b}} + \hat{C}_{S,\beta}\beta_{,V_{x_b}} + \hat{C}_{S,L\bar{p}}\hat{C}_{L,\alpha}\alpha_{,V_{x_b}}\bar{p} + \left(\hat{C}_{S,L\bar{p}}\hat{C}_{L_1} + \hat{C}_{S,\bar{p}}\right)\bar{p}_{,V_{x_b}} + \hat{C}_{S,\bar{q}}\bar{q}_{,V_{x_b}} + \hat{C}_{S,\bar{r}}\bar{r}_{,V_{x_b}} \tag{B.50}$$

$$\mathring{C}_{S,V_{y_b}} = \hat{C}_{S,\beta}\beta_{,V_{y_b}} + \left(\hat{C}_{S,L\bar{p}}\hat{C}_{L_1} + \hat{C}_{S,\bar{p}}\right)\bar{p}_{,V_{y_b}} + \hat{C}_{S,\bar{q}}\bar{q}_{,V_{y_b}} + \hat{C}_{S,\bar{r}}\bar{r}_{,V_{y_b}} \tag{B.51}$$

$$\mathring{C}_{S,V_{z_b}} = \hat{C}_{S,\alpha}\alpha_{,V_{z_b}} + \hat{C}_{S,\beta}\beta_{,V_{z_b}} + \hat{C}_{S,L\bar{p}}\hat{C}_{L,\alpha}\alpha_{,V_{z_b}}\bar{p} + \left(\hat{C}_{S,L\bar{p}}\hat{C}_{L_1} + \hat{C}_{S,\bar{p}}\right)\bar{p}_{,V_{z_b}} + \hat{C}_{S,\bar{q}}\bar{q}_{,V_{z_b}} + \hat{C}_{S,\bar{r}}\bar{r}_{,V_{z_b}} \tag{B.52}$$

$$\mathring{C}_{S,p} = \left(\hat{C}_{S,L\bar{p}}\hat{C}_{L_1} + \hat{C}_{S,\bar{p}}\right)R_{lat} \tag{B.53}$$

$$\mathring{C}_{S,q} = \hat{C}_{S,\bar{q}}R_{lon} \tag{B.54}$$

$$\mathring{C}_{S,r} = \hat{C}_{S,\bar{r}}R_{lat} \tag{B.55}$$

The derivatives of drag coefficient with respect to state are

$$\begin{aligned}\mathring{C}_{D,V_{x_b}} = {} & \left(\hat{C}_{D,L} + 2\hat{C}_{D,L^2}\hat{C}_{L_1} + \left(2\hat{C}_{D,L^2\bar{q}}\hat{C}_{L_1} + \hat{C}_{D,L\bar{q}}\right)\bar{q} + \hat{C}_{D,L\delta_e}\delta_e\right)\hat{C}_{L,\alpha}\alpha_{,V_{x_b}} \\ & + \left(\hat{C}_{D,S} + 2\hat{C}_{D,S^2}\hat{C}_{S_1} + \hat{C}_{D,S\bar{p}}\bar{p} + \hat{C}_{D,S\bar{r}}\bar{r} + \hat{C}_{D,S\delta_a}\delta_a\right)\hat{C}_{S,\beta}\beta_{,V_{x_b}} \\ & + \left(\hat{C}_{D,S\bar{p}}\hat{C}_{S_1} + \hat{C}_{D,\bar{p}}\right)\bar{p}_{,V_{x_b}} + \left(\hat{C}_{D,L^2\bar{q}}\hat{C}_{L_1}^2 + \hat{C}_{D,L\bar{q}}\hat{C}_{L_1} + \hat{C}_{D,\bar{q}}\right)\bar{q}_{,V_{x_b}} + \left(\hat{C}_{D,S\bar{r}}\hat{C}_{S_1} + \hat{C}_{D,\bar{r}}\right)\bar{r}_{,V_{x_b}}\end{aligned} \tag{B.56}$$

$$\begin{aligned}\mathring{C}_{D,V_{y_b}} = {} & \left(\hat{C}_{D,S} + 2\hat{C}_{D,S^2}\hat{C}_{S_1} + \hat{C}_{D,S\bar{p}}\bar{p} + \hat{C}_{D,S\bar{r}}\bar{r} + \hat{C}_{D,S\delta_a}\delta_a\right)\hat{C}_{S,\beta}\beta_{,V_{y_b}} \\ & + \left(\hat{C}_{D,S\bar{p}}\hat{C}_{S_1} + \hat{C}_{D,\bar{p}}\right)\bar{p}_{,V_{y_b}} + \left(\hat{C}_{D,L^2\bar{q}}\hat{C}_{L_1}^2 + \hat{C}_{D,L\bar{q}}\hat{C}_{L_1} + \hat{C}_{D,\bar{q}}\right)\bar{q}_{,V_{y_b}} + \left(\hat{C}_{D,S\bar{r}}\hat{C}_{S_1} + \hat{C}_{D,\bar{r}}\right)\bar{r}_{,V_{y_b}}\end{aligned} \tag{B.57}$$

$$\begin{aligned}\mathring{C}_{D,V_{z_b}} = {} & \left(\hat{C}_{D,L} + 2\hat{C}_{D,L^2}\hat{C}_{L_1} + \left(2\hat{C}_{D,L^2\bar{q}}\hat{C}_{L_1} + \hat{C}_{D,L\bar{q}}\right)\bar{q} + \hat{C}_{D,L\delta_e}\delta_e\right)\hat{C}_{L,\alpha}\alpha_{,V_{z_b}} \\ & + \left(\hat{C}_{D,S} + 2\hat{C}_{D,S^2}\hat{C}_{S_1} + \hat{C}_{D,S\bar{p}}\bar{p} + \hat{C}_{D,S\bar{r}}\bar{r} + \hat{C}_{D,S\delta_a}\delta_a\right)\hat{C}_{S,\beta}\beta_{,V_{z_b}} \\ & + \left(\hat{C}_{D,S\bar{p}}\hat{C}_{S_1} + \hat{C}_{D,\bar{p}}\right)\bar{p}_{,V_{z_b}} + \left(\hat{C}_{D,L^2\bar{q}}\hat{C}_{L_1}^2 + \hat{C}_{D,L\bar{q}}\hat{C}_{L_1} + \hat{C}_{D,\bar{q}}\right)\bar{q}_{,V_{z_b}} + \left(\hat{C}_{D,S\bar{r}}\hat{C}_{S_1} + \hat{C}_{D,\bar{r}}\right)\bar{r}_{,V_{z_b}}\end{aligned} \tag{B.58}$$

$$\mathring{C}_{D,p} = \left(\hat{C}_{D,S\bar{p}}\hat{C}_{S_1} + \hat{C}_{D,\bar{p}}\right)R_{lat} \tag{B.59}$$

$$\mathring{C}_{D,q} = \left(\hat{C}_{D,L^2\bar{q}}\hat{C}_{L_1}^2 + \hat{C}_{D,L\bar{q}}\hat{C}_{L_1} + \hat{C}_{D,\bar{q}}\right)R_{lon} \tag{B.60}$$

$$\mathring{C}_{D,r} = \left(\hat{C}_{D,S\bar{r}}\hat{C}_{S_1} + \hat{C}_{D,\bar{r}}\right)R_{lat} \tag{B.61}$$

The derivatives of rolling moment coefficient with respect to state are

$$\mathring{C}_{\ell,V_{x_b}} = \hat{C}_{\ell,\alpha}\alpha_{,V_{x_b}} + \hat{C}_{\ell,\beta}\beta_{,V_{x_b}} + \hat{C}_{\ell,\bar{p}}\bar{p}_{,V_{x_b}} + \hat{C}_{\ell,\bar{q}}\bar{q}_{,V_{x_b}} + \hat{C}_{\ell,L\bar{r}}\hat{C}_{L,\alpha}\alpha_{,V_{x_b}}\bar{r} + \left(\hat{C}_{\ell,L\bar{r}}\hat{C}_{L_1} + \hat{C}_{\ell,\bar{r}}\right)\bar{r}_{,V_{x_b}} \tag{B.62}$$

$$\mathring{C}_{\ell,V_{y_b}} = \hat{C}_{\ell,\beta}\beta_{,V_{y_b}} + \hat{C}_{\ell,\bar{p}}\bar{p}_{,V_{y_b}} + \hat{C}_{\ell,\bar{q}}\bar{q}_{,V_{y_b}} + \left(\hat{C}_{\ell,L\bar{r}}\hat{C}_{L_1} + \hat{C}_{\ell,\bar{r}}\right)\bar{r}_{,V_{y_b}} \tag{B.63}$$

$$\mathring{C}_{\ell,V_{z_b}} = \hat{C}_{\ell,\alpha}\alpha_{,V_{z_b}} + \hat{C}_{\ell,\beta}\beta_{,V_{z_b}} + \hat{C}_{\ell,\bar{p}}\bar{p}_{,V_{z_b}} + \hat{C}_{\ell,\bar{q}}\bar{q}_{,V_{z_b}} + \hat{C}_{\ell,L\bar{r}}\hat{C}_{L,\alpha}\alpha_{,V_{z_b}}\bar{r} + \left(\hat{C}_{\ell,L\bar{r}}\hat{C}_{L_1} + \hat{C}_{\ell,\bar{r}}\right)\bar{r}_{,V_{z_b}} \tag{B.64}$$

$$\mathring{C}_{\ell,p} = \hat{C}_{\ell,\bar{p}}R_{lat} \tag{B.65}$$

$$\mathring{C}_{\ell,q} = \hat{C}_{\ell,\bar{q}}R_{lon} \tag{B.66}$$

$$\mathring{C}_{\ell,r} = \left(\hat{C}_{\ell,L\bar{r}}\hat{C}_{L_1} + \hat{C}_{\ell,\bar{r}}\right)R_{lat} \tag{B.67}$$

The derivatives of pitching moment coefficient with respect to state are

$$\mathring{C}_{m,V_{x_b}} = \hat{C}_{m,\alpha}\alpha_{,V_{x_b}} + \hat{C}_{m,\beta}\beta_{,V_{x_b}} + \hat{C}_{m,\bar{p}}\bar{p}_{,V_{x_b}} + \hat{C}_{m,\bar{q}}\bar{q}_{,V_{x_b}} + \hat{C}_{m,\bar{r}}\bar{r}_{,V_{x_b}} \tag{B.68}$$

$$\mathring{C}_{m,V_{y_b}} = \hat{C}_{m,\beta}\beta_{,V_{y_b}} + \hat{C}_{m,\bar{p}}\bar{p}_{,V_{y_b}} + \hat{C}_{m,\bar{q}}\bar{q}_{,V_{y_b}} + \hat{C}_{m,\bar{r}}\bar{r}_{,V_{y_b}} \tag{B.69}$$

$$\mathring{C}_{m,V_{z_b}} = \hat{C}_{m,\alpha}\alpha_{,V_{z_b}} + \hat{C}_{m,\beta}\beta_{,V_{z_b}} + \hat{C}_{m,\bar{p}}\bar{p}_{,V_{z_b}} + \hat{C}_{m,\bar{q}}\bar{q}_{,V_{z_b}} + \hat{C}_{m,\bar{r}}\bar{r}_{,V_{z_b}} \tag{B.70}$$

$$\mathring{C}_{m,p} = \hat{C}_{m,\bar{p}}R_{lat} \tag{B.71}$$

$$\mathring{C}_{m,q} = \hat{C}_{m,\bar{q}}R_{lon} \tag{B.72}$$

$$\mathring{C}_{m,r} = \hat{C}_{m,\bar{r}}R_{lat} \tag{B.73}$$

The derivatives of yawing moment coefficient with respect to state are

$$\mathring{C}_{n,V_{x_b}} = \left[\left(\hat{C}_{n,L\bar{p}}\bar{p} + \hat{C}_{n,L\delta_a}\delta_a\right)\hat{C}_{L,\alpha} + \hat{C}_{n,\alpha}\right]\alpha_{,V_{x_b}} + \hat{C}_{n,\beta}\beta_{,V_{x_b}} + \left(\hat{C}_{n,L\bar{p}}\hat{C}_{L_1} + \hat{C}_{n,\bar{p}}\right)\bar{p}_{,V_{x_b}} + \hat{C}_{n,\bar{q}}\bar{q}_{,V_{x_b}} + \hat{C}_{n,\bar{r}}\bar{r}_{,V_{x_b}} \tag{B.74}$$

$$\mathring{C}_{n,V_{y_b}} = \hat{C}_{n,\beta}\beta_{,V_{y_b}} + \left(\hat{C}_{n,L\bar{p}}\hat{C}_{L_1} + \hat{C}_{n,\bar{p}}\right)\bar{p}_{,V_{y_b}} + \hat{C}_{n,\bar{q}}\bar{q}_{,V_{y_b}} + \hat{C}_{n,\bar{r}}\bar{r}_{,V_{y_b}} \tag{B.75}$$

$$\mathring{C}_{n,V_{z_b}} = \left[\left(\hat{C}_{n,L\bar{p}}\bar{p} + \hat{C}_{n,L\delta_a}\delta_a\right)\hat{C}_{L,\alpha} + \hat{C}_{n,\alpha}\right]\alpha_{,V_{z_b}} + \hat{C}_{n,\beta}\beta_{,V_{z_b}} + \left(\hat{C}_{n,L\bar{p}}\hat{C}_{L_1} + \hat{C}_{n,\bar{p}}\right)\bar{p}_{,V_{z_b}} + \hat{C}_{n,\bar{q}}\bar{q}_{,V_{z_b}} + \hat{C}_{n,\bar{r}}\bar{r}_{,V_{z_b}} \tag{B.76}$$

$$\mathring{C}_{n,p} = \left(\hat{C}_{n,L\bar{p}}\hat{C}_{L_1} + \hat{C}_{n,\bar{p}}\right)R_{lat} \tag{B.77}$$

$$\mathring{C}_{n,q} = \hat{C}_{n,\bar{q}}R_{lon} \tag{B.78}$$

$$\mathring{C}_{n,r} = \hat{C}_{n,\bar{r}}R_{lat} \tag{B.79}$$

D. BIRE Aerodynamic Force and Moment Derivatives with respect to Input

The aerodynamic force and moment derivatives with respect to input will now be found for the BIRE. The coefficient derivatives with respect to BIRE angle will be denoted as

$$\breve{C} = A\omega\cos\left(\omega\delta_B + \phi\right) \tag{B.80}$$

The derivatives of lift coefficient with respect to input are

$$\mathring{C}_{L,\delta_B} = \breve{C}_{L_0} + \breve{C}_{L,\alpha}\alpha + \breve{C}_{L,\beta}\beta + \breve{C}_{L,\bar{p}}\bar{p} + \breve{C}_{L,\bar{q}}\bar{q} + \breve{C}_{L,\bar{r}}\bar{r} + \breve{C}_{L,\delta_a}\delta_a + \breve{C}_{L,\delta_e^B}\delta_e^B \tag{B.81}$$

The derivatives of side-force coefficient with respect to input are

$$\mathring{C}_{S,\delta_B} = \breve{C}_{S_0} + \breve{C}_{S,\alpha}\alpha + \breve{C}_{S,\beta}\beta + \left(\breve{C}_{S,L\bar{p}}\hat{C}_{L_1} + \hat{C}_{S,L\bar{p}}\breve{C}_{L_1} + \breve{C}_{S,\bar{p}}\right)\bar{p} + \breve{C}_{S,\bar{q}}\bar{q} + \breve{C}_{S,\bar{r}}\bar{r} + \breve{C}_{S,\delta_a}\delta_a + \breve{C}_{S,\delta_e^B}\delta_e^B \tag{B.82}$$

The derivatives of drag coefficient with respect to input are

$$\mathring{C}_{D,\delta_a} = \hat{C}_{D,S\delta_a}\hat{C}_{S_1} + \hat{C}_{D,\delta_a} \tag{B.83}$$

$$\mathring{C}_{D,\delta_e} = \mathring{C}_{D,\delta_e^B} = \hat{C}_{D,L\delta_e^B}\hat{C}_{L_1} + \hat{C}_{D,\delta_e^B} + 2\hat{C}_{D,\delta_e^{B\,2}}\delta_e^B \tag{B.84}$$

$$\begin{aligned}\mathring{C}_{D,\delta_B} = {} & \breve{C}_{D_0} + \breve{C}_{D,L}\hat{C}_{L_1} + \hat{C}_{D,L}\breve{C}_{L_1} + \breve{C}_{D,L^2}\hat{C}_{L_1}^2 + 2\hat{C}_{D,L^2}\hat{C}_{L_1}\breve{C}_{L_1} \\ & + \breve{C}_{D,S}\hat{C}_{S_1} + \hat{C}_{D,S}\breve{C}_{S_1} + \breve{C}_{D,S^2}\hat{C}_{S_1}^2 + 2\hat{C}_{D,S^2}\hat{C}_{S_1}\breve{C}_{S_1} \\ & + \left(\breve{C}_{D,S\bar{p}}\hat{C}_{S_1} + \hat{C}_{D,S\bar{p}}\breve{C}_{S_1} + \breve{C}_{D,\bar{p}}\right)\bar{p} \\ & + \left(\breve{C}_{D,L^2\bar{q}}\hat{C}_{L_1}^2 + 2\hat{C}_{D,L^2\bar{q}}\hat{C}_{L_1}\breve{C}_{L_1} + \breve{C}_{D,L\bar{q}}\hat{C}_{L_1} + \hat{C}_{D,L\bar{q}}\breve{C}_{L_1} + \breve{C}_{D,\bar{q}}\right)\bar{q} \\ & + \left(\breve{C}_{D,S\bar{r}}\hat{C}_{S_1} + \hat{C}_{D,S\bar{r}}\breve{C}_{S_1} + \breve{C}_{D,\bar{r}}\right)\bar{r} \\ & + \left(\breve{C}_{D,S\delta_a}\hat{C}_{S_1} + \hat{C}_{D,S\delta_a}\breve{C}_{S_1} + \breve{C}_{D,\delta_a}\right)\delta_a + \left(\breve{C}_{D,L\delta_e^B}\hat{C}_{L_1} + \hat{C}_{D,L\delta_e^B}\breve{C}_{L_1} + \breve{C}_{D,\delta_e^B}\right)\delta_e^B + \breve{C}_{D,\delta_e^{B\,2}}\delta_e^{B\,2}\end{aligned} \tag{B.85}$$

The derivatives of rolling moment coefficient with respect to input are

$$\mathring{C}_{\ell,\delta_B} = \breve{C}_{\ell_0} + \breve{C}_{\ell,\alpha}\alpha + \breve{C}_{\ell,\beta}\beta + \breve{C}_{\ell,\bar{p}}\bar{p} + \breve{C}_{\ell,\bar{q}}\bar{q} + \left(\breve{C}_{\ell,L\bar{r}}\hat{C}_{L_1} + \hat{C}_{\ell,L\bar{r}}\breve{C}_{L_1} + \breve{C}_{\ell,\bar{r}}\right)\bar{r} + \breve{C}_{\ell,\delta_a}\delta_a + \breve{C}_{\ell,\delta_e^B}\delta_e^B \tag{B.86}$$

The derivatives of pitching moment coefficient with respect to input are

$$\mathring{C}_{m,\delta_B} = \breve{C}_{m_0} + \breve{C}_{m,\alpha}\alpha + \breve{C}_{m,\beta}\beta + \breve{C}_{m,\bar{p}}\bar{p} + \breve{C}_{m,\bar{q}}\bar{q} + \breve{C}_{m,\bar{r}}\bar{r} + \breve{C}_{m,\delta_a}\delta_a + \breve{C}_{m,\delta_e^B}\delta_e^B \tag{B.87}$$

The derivatives of yawing moment coefficient with respect to input are

$$\mathring{C}_{n,\delta_a} = \hat{C}_{n,L\delta_a}\hat{C}_{L_1} + \hat{C}_{n,\delta_a} \tag{B.88}$$

$$\begin{aligned}\mathring{C}_{n,\delta_B} = {} & \breve{C}_{n_0} + \breve{C}_{n,\alpha}\alpha + \breve{C}_{n,\beta}\beta + \left(\breve{C}_{n,L\bar{p}}\hat{C}_{L_1} + \hat{C}_{n,L\bar{p}}\breve{C}_{L_1} + \breve{C}_{n,\bar{p}}\right)\bar{p} \\ & + \breve{C}_{n,\bar{q}}\bar{q} + \breve{C}_{n,\bar{r}}\bar{r} + \left(\breve{C}_{n,L\delta_a}\hat{C}_{L_1} + \hat{C}_{n,L\delta_a}\breve{C}_{L_1} + \breve{C}_{n,\delta_a}\right)\delta_a + \breve{C}_{n,\delta_e^B}\delta_e^B\end{aligned} \tag{B.89}$$

where

$$\breve{C}_{L_1} = \breve{C}_{L_0} + \breve{C}_{L,\alpha}\alpha \tag{B.90}$$

$$\breve{C}_{S_1} = \breve{C}_{S_0} + \breve{C}_{S,\beta}\beta \tag{B.91}$$

The following coefficients are equivalent to the BIRE-angle dependant coefficients shown in the aerodynamic model given in Eqs. (18) – (25) (i.e. $\mathring{C}_{L,\delta_e} = \mathring{C}_{L,\delta_e^B} = \hat{C}_{L,\delta_e^B}$)

$$\mathring{C}_{L,\delta_a}, \mathring{C}_{L,\delta_e}, \mathring{C}_{S,\delta_a}, \mathring{C}_{S,\delta_e}, \mathring{C}_{\ell,\delta_a}, \mathring{C}_{\ell,\delta_e}, \mathring{C}_{m,\delta_a}, \mathring{C}_{m,\delta_e}, \mathring{C}_{n,\delta_e} \tag{B.92}$$

E. Stall Derivatives

As the evaluated trim condition of the aircraft is in steady level flight, well within the linear region of lift, the stall derivatives are neglected from this formulation (i.e. $\acute{C}_{A,v} = \mathring{C}_{A,v}$).

F. Compressibility Derivatives

Each of the incompressible derivatives given previously can be corrected for compressibility. The derivative of an incompressible force or moment $\acute{C}_A$ with respect to a given state or input component v can be corrected for compressibility using the chain rule as

$$C_{A,v} = C_{A,\acute{C}_A}\acute{C}_{A,v} + C_{A,M}M_{,v} \tag{B.93}$$

where

$$C_{A,\acute{C}_A} = \frac{\cos\Lambda_{c/2}\left(\pi R_A\sqrt{1 - M^2\cos^2\Lambda_{c/2} + \left[\frac{\acute{C}_A\cos\Lambda_{c/2}}{(\pi R_A)}\right]^2} - \acute{C}_A\cos\Lambda_{c/2}\right)}{\acute{C}_A\cos\Lambda_{c/2}\sqrt{1 - M^2\cos^2\Lambda_{c/2} + \left[\frac{\acute{C}_A\cos\Lambda_{c/2}}{(\pi R_A)}\right]^2} + \pi R_A\left(1 - M^2\cos^2\Lambda_{c/2} + \left[\frac{\acute{C}_A\cos\Lambda_{c/2}}{(\pi R_A)}\right]^2\right)} \tag{B.94}$$

$$C_{A,M} = \frac{\acute{C}_A\cos\Lambda_{c/2}}{\frac{\acute{C}_A\cos\Lambda_{c/2}}{(\pi R_A)}\sqrt{1 - M^2\cos^2\Lambda_{c/2} + \left[\frac{\acute{C}_A\cos\Lambda_{c/2}}{(\pi R_A)}\right]^2} + 1 - M^2\cos^2\Lambda_{c/2} + \left[\frac{\acute{C}_A\cos\Lambda_{c/2}}{(\pi R_A)}\right]^2} \tag{B.95}$$

and

$$M_{,V_{x_b}} = \frac{2V_{x_b}}{Va}, \quad M_{,V_{y_b}} = \frac{2V_{y_b}}{Va}, \quad M_{,V_{z_b}} = \frac{2V_{z_b}}{Va} \tag{B.96}$$

$$M_{,p} = M_{,q} = M_{,r} = M_{,\delta_a} = M_{,\delta_e} = M_{,\delta_r} = M_{,\delta_B} = M_{,\tau} = 0 \tag{B.97}$$

G. Propulsion Force Derivatives with respect to State

The state derivatives of the thrust model are

$$T_{,V} = \begin{cases} T_{\text{idle},V} + (T_{\text{mil},V} - T_{\text{idle},V})\frac{P_1}{50}, & P_1 < 50 \\ T_{\text{mil},V} + (T_{\text{max},V} - T_{\text{mil},V})\frac{P_1-50}{50}, & P_1 \geq 50 \end{cases} \tag{B.98}$$

$$T_{\text{set},V} = \left(\frac{\rho}{\rho_0}\right)^{a_{\text{set}}} (T_{\text{set}\,1} + 2T_{\text{set}\,2}V) \tag{B.99}$$

Note, the effect of Earth-fixed altitude state (z_f) on freestream air density and thrust model parameters was assumed to be minor, and is neglected in this formulation.

H. Propulsion Force Derivatives with respect to Input

The input derivatives of the thrust model are

$$T_{,\tau} = \begin{cases} (T_{\text{mil}} - T_{\text{idle}})\frac{P_{1,\tau}}{50}, & \tau \leq 0.77 \\ (T_{\text{max}} - T_{\text{mil}})\frac{P_{1,\tau}}{50}, & \tau > 0.77 \end{cases} \tag{B.100}$$

$$P_{1,\tau} = \begin{cases} 64.94, & \tau \leq 0.77 \\ 217.38, & \tau > 0.77 \end{cases} \tag{B.101}$$

I. Body-Fixed Force and Moment Derivatives with respect to State

The body-fixed force and moment derivatives with respect to state will be found using the defined aerodynamic force and moment derivatives with respect to state given previously for the baseline or BIRE. Note, these equations apply to either aircraft. The derivatives of the body-fixed x-force with respect to state are

$$\begin{aligned} F_{x_b,V_{x_b}} &= \rho S_w V_{x_b}\left(C_L S_\alpha - C_S C_\alpha S_\beta - C_D C_\alpha C_\beta\right) \\ &\quad + \frac{1}{2}\rho V^2 S_w \Big(C_{L,V_{x_b}} S_\alpha + C_L C_\alpha \alpha_{,V_{x_b}} - C_{S,V_{x_b}} C_\alpha S_\beta + C_S S_\alpha S_\beta \alpha_{,V_{x_b}} - C_S C_\alpha C_\beta \beta_{,V_{x_b}} \\ &\qquad - C_{D,V_{x_b}} C_\alpha C_\beta + C_D S_\alpha C_\beta \alpha_{,V_{x_b}} + C_D C_\alpha S_\beta \beta_{,V_{x_b}}\Big) + T_{,V}\frac{V_{x_b}}{V} \end{aligned} \tag{B.102}$$

$$\begin{aligned} F_{x_b,V_{y_b}} &= \rho S_w V_{y_b}\left(C_L S_\alpha - C_S C_\alpha S_\beta - C_D C_\alpha C_\beta\right) \\ &\quad + \frac{1}{2}\rho V^2 S_w \Big(C_{L,V_{y_b}} S_\alpha - C_{S,V_{y_b}} C_\alpha S_\beta - C_S C_\alpha C_\beta \beta_{,V_{y_b}} \\ &\qquad - C_{D,V_{y_b}} C_\alpha C_\beta + C_D C_\alpha S_\beta \beta_{,V_{y_b}}\Big) + T_{,V}\frac{V_{y_b}}{V} \end{aligned} \tag{B.103}$$

$$\begin{aligned} F_{x_b,V_{z_b}} &= \rho S_w V_{z_b}\left(C_L S_\alpha - C_S C_\alpha S_\beta - C_D C_\alpha C_\beta\right) \\ &\quad + \frac{1}{2}\rho V^2 S_w \Big(C_{L,V_{z_b}} S_\alpha + C_L C_\alpha \alpha_{,V_{z_b}} - C_{S,V_{z_b}} C_\alpha S_\beta + C_S S_\alpha S_\beta \alpha_{,V_{z_b}} - C_S C_\alpha C_\beta \beta_{,V_{z_b}} \\ &\qquad - C_{D,V_{z_b}} C_\alpha C_\beta + C_D S_\alpha C_\beta \alpha_{,V_{z_b}} + C_D C_\alpha S_\beta \beta_{,V_{z_b}}\Big) + T_{,V}\frac{V_{z_b}}{V} \end{aligned} \tag{B.104}$$

$$F_{x_b,p} = \frac{1}{2}\rho V^2 S_w \left(C_{L,p} S_\alpha - C_{S,p} C_\alpha S_\beta - C_{D,p} C_\alpha C_\beta\right) \tag{B.105}$$

$$F_{x_b,q} = \frac{1}{2}\rho V^2 S_w \left(C_{L,q} S_\alpha - C_{S,q} C_\alpha S_\beta - C_{D,q} C_\alpha C_\beta\right) \tag{B.106}$$

$$F_{x_b,r} = \frac{1}{2}\rho V^2 S_w \left(C_{L,r} S_\alpha - C_{S,r} C_\alpha S_\beta - C_{D,r} C_\alpha C_\beta\right) \tag{B.107}$$

The derivatives of the body-fixed y-force with respect to state are

$$F_{y_b,V_{x_b}} = \rho S_w V_{x_b}\left(C_S C_\beta - C_D S_\beta\right) + \frac{1}{2}\rho V^2 S_w \left(C_{S,V_{x_b}} C_\beta - C_S S_\beta \beta_{,V_{x_b}} - C_{D,V_{x_b}} S_\beta - C_D C_\beta \beta_{,V_{x_b}}\right) \tag{B.108}$$

$$F_{y_b,V_{y_b}} = \rho S_w V_{y_b} \left(C_S C_\beta - C_D S_\beta\right) + \frac{1}{2}\rho V^2 S_w \left(C_{S,V_{y_b}} C_\beta - C_S S_\beta \beta_{,V_{y_b}} - C_{D,V_{y_b}} S_\beta - C_D C_\beta \beta_{,V_{y_b}}\right) \tag{B.109}$$

$$F_{y_b,V_{z_b}} = \rho S_w V_{z_b} \left(C_S C_\beta - C_D S_\beta\right) + \frac{1}{2}\rho V^2 S_w \left(C_{S,V_{z_b}} C_\beta - C_S S_\beta \beta_{,V_{z_b}} - C_{D,V_{z_b}} S_\beta - C_D C_\beta \beta_{,V_{z_b}}\right) \tag{B.110}$$

$$F_{y_b,p} = \frac{1}{2}\rho V^2 S_w \left(C_{S,p} C_\beta - C_{D,p} S_\beta\right) \tag{B.111}$$

$$F_{y_b,q} = \frac{1}{2}\rho V^2 S_w \left(C_{S,q} C_\beta - C_{D,q} S_\beta\right) \tag{B.112}$$

$$F_{y_b,r} = \frac{1}{2}\rho V^2 S_w \left(C_{S,r} C_\beta - C_{D,r} S_\beta\right) \tag{B.113}$$

The derivatives of the body-fixed z-force with respect to state are

$$\begin{aligned} F_{z_b,V_{x_b}} &= \rho S_w V_{x_b} \left(-C_L C_\alpha - C_S S_\alpha S_\beta - C_D S_\alpha C_\beta\right) \\ &\quad + \frac{1}{2}\rho V^2 S_w \left(-C_{L,V_{x_b}} C_\alpha + C_L S_\alpha \alpha_{,V_{x_b}} - C_{S,V_{x_b}} S_\alpha S_\beta - C_S C_\alpha S_\beta \alpha_{,V_{x_b}} - C_S S_\alpha C_\beta \beta_{,V_{x_b}}\right. \\ &\qquad \left. - C_{D,V_{x_b}} S_\alpha C_\beta - C_D C_\alpha C_\beta \alpha_{,V_{x_b}} + C_D S_\alpha S_\beta \beta_{,V_{x_b}}\right) \end{aligned} \tag{B.114}$$

$$\begin{aligned} F_{z_b,V_{y_b}} &= \rho S_w V_{y_b} \left(-C_L C_\alpha - C_S S_\alpha S_\beta - C_D S_\alpha C_\beta\right) \\ &\quad + \frac{1}{2}\rho V^2 S_w \left(-C_{L,V_{y_b}} C_\alpha - C_{S,V_{y_b}} S_\alpha S_\beta - C_S S_\alpha C_\beta \beta_{,V_{y_b}}\right. \\ &\qquad \left. - C_{D,V_{y_b}} S_\alpha C_\beta + C_D S_\alpha S_\beta \beta_{,V_{y_b}}\right) \end{aligned} \tag{B.115}$$

$$\begin{aligned} F_{z_b,V_{z_b}} &= \rho S_w V_{z_b} \left(-C_L C_\alpha - C_S S_\alpha S_\beta - C_D S_\alpha C_\beta\right) \\ &\quad + \frac{1}{2}\rho V^2 S_w \left(-C_{L,V_{z_b}} C_\alpha + C_L S_\alpha \alpha_{,V_{z_b}} - C_{S,V_{z_b}} S_\alpha S_\beta - C_S C_\alpha S_\beta \alpha_{,V_{z_b}} - C_S S_\alpha C_\beta \beta_{,V_{z_b}}\right. \\ &\qquad \left. - C_{D,V_{z_b}} S_\alpha C_\beta - C_D C_\alpha C_\beta \alpha_{,V_{z_b}} + C_D S_\alpha S_\beta \beta_{,V_{z_b}}\right) \end{aligned} \tag{B.116}$$

$$F_{z_b,p} = \frac{1}{2}\rho V^2 S_w \left(-C_{L,p} C_\alpha - C_{S,p} S_\alpha S_\beta - C_{D,p} S_\alpha C_\beta\right) \tag{B.117}$$

$$F_{z_b,q} = \frac{1}{2}\rho V^2 S_w \left(-C_{L,q} C_\alpha - C_{S,q} S_\alpha S_\beta - C_{D,q} S_\alpha C_\beta\right) \tag{B.118}$$

$$F_{z_b,r} = \frac{1}{2}\rho V^2 S_w \left(-C_{L,r} C_\alpha - C_{S,r} S_\alpha S_\beta - C_{D,r} S_\alpha C_\beta\right) \tag{B.119}$$

The moment derivatives are performed on equations formulated to include an offset in the center of gravity, as

$$\begin{bmatrix} M_{x_b} \\ M_{y_b} \\ M_{z_b} \end{bmatrix} = \frac{1}{2}\rho V^2 S_w \begin{bmatrix} b_w C_\ell \\ \bar{c}_w C_m \\ b_w C_n \end{bmatrix} + \begin{bmatrix} F_{x_b} \\ F_{y_b} \\ F_{z_b} \end{bmatrix} \times \begin{bmatrix} \Delta x_{cg} \\ \Delta y_{cg} \\ \Delta z_{cg} \end{bmatrix}$$

The derivatives of the body-fixed x-moment with respect to state are

$$M_{x_b,V_{x_b}} = \rho S_w b_w V_{x_b} C_\ell + \frac{1}{2}\rho V^2 S_w b_w C_{\ell,V_{x_b}} + F_{y_b,V_{x_b}} \Delta z_{cg} - F_{z_b,V_{x_b}} \Delta y_{cg} \tag{B.120}$$

$$M_{x_b,V_{y_b}} = \rho S_w b_w V_{y_b} C_\ell + \frac{1}{2}\rho V^2 S_w b_w C_{\ell,V_{y_b}} + F_{y_b,V_{y_b}} \Delta z_{cg} - F_{z_b,V_{y_b}} \Delta y_{cg} \tag{B.121}$$

$$M_{x_b,V_{z_b}} = \rho S_w b_w V_{z_b} C_\ell + \frac{1}{2}\rho V^2 S_w b_w C_{\ell,V_{z_b}} + F_{y_b,V_{z_b}} \Delta z_{cg} - F_{z_b,V_{z_b}} \Delta y_{cg} \tag{B.122}$$

$$M_{x_b,p} = \frac{1}{2}\rho V^2 S_w b_w C_{\ell,p} + F_{y_b,p} \Delta z_{cg} - F_{z_b,p} \Delta y_{cg} \tag{B.123}$$

$$M_{x_b,q} = \frac{1}{2}\rho V^2 S_w b_w C_{\ell,q} + F_{y_b,q}\Delta z_{cg} - F_{z_b,q}\Delta y_{cg} \tag{B.124}$$

$$M_{x_b,r} = \frac{1}{2}\rho V^2 S_w b_w C_{\ell,r} + F_{y_b,r}\Delta z_{cg} - F_{z_b,r}\Delta y_{cg} \tag{B.125}$$

The derivatives of the body-fixed y-moment with respect to state are

$$M_{y_b,V_{x_b}} = \rho S_w \bar{c}_w V_{x_b} C_m + \frac{1}{2}\rho V^2 S_w \bar{c}_w C_{m,V_{x_b}} + F_{z_b,V_{x_b}}\Delta x_{cg} - F_{x_b,V_{x_b}}\Delta z_{cg} \tag{B.126}$$

$$M_{y_b,V_{y_b}} = \rho S_w \bar{c}_w V_{y_b} C_m + \frac{1}{2}\rho V^2 S_w \bar{c}_w C_{m,V_{y_b}} + F_{z_b,V_{y_b}}\Delta x_{cg} - F_{x_b,V_{y_b}}\Delta z_{cg} \tag{B.127}$$

$$M_{y_b,V_{z_b}} = \rho S_w \bar{c}_w V_{z_b} C_m + \frac{1}{2}\rho V^2 S_w \bar{c}_w C_{m,V_{z_b}} + F_{z_b,V_{z_b}}\Delta x_{cg} - F_{x_b,V_{z_b}}\Delta z_{cg} \tag{B.128}$$

$$M_{y_b,p} = \frac{1}{2}\rho V^2 S_w \bar{c}_w C_{m,p} + F_{z_b,p}\Delta x_{cg} - F_{x_b,p}\Delta z_{cg} \tag{B.129}$$

$$M_{y_b,q} = \frac{1}{2}\rho V^2 S_w \bar{c}_w C_{m,q} + F_{z_b,q}\Delta x_{cg} - F_{x_b,q}\Delta z_{cg} \tag{B.130}$$

$$M_{y_b,r} = \frac{1}{2}\rho V^2 S_w \bar{c}_w C_{m,r} + F_{z_b,r}\Delta x_{cg} - F_{x_b,r}\Delta z_{cg} \tag{B.131}$$

The derivatives of the body-fixed z-moment with respect to state are

$$M_{z_b,V_{x_b}} = \rho S_w b_w V_{x_b} C_n + \frac{1}{2}\rho V^2 S_w b_w C_{n,V_{x_b}} + F_{x_b,V_{x_b}}\Delta y_{cg} - F_{y_b,V_{x_b}}\Delta x_{cg} \tag{B.132}$$

$$M_{z_b,V_{y_b}} = \rho S_w b_w V_{y_b} C_n + \frac{1}{2}\rho V^2 S_w b_w C_{n,V_{y_b}} + F_{x_b,V_{y_b}}\Delta y_{cg} - F_{y_b,V_{y_b}}\Delta x_{cg} \tag{B.133}$$

$$M_{z_b,V_{z_b}} = \rho S_w b_w V_{z_b} C_n + \frac{1}{2}\rho V^2 S_w b_w C_{n,V_{z_b}} + F_{x_b,V_{z_b}}\Delta y_{cg} - F_{y_b,V_{z_b}}\Delta x_{cg} \tag{B.134}$$

$$M_{z_b,p} = \frac{1}{2}\rho V^2 S_w b_w C_{n,p} + F_{x_b,p}\Delta y_{cg} - F_{y_b,p}\Delta x_{cg} \tag{B.135}$$

$$M_{z_b,q} = \frac{1}{2}\rho V^2 S_w b_w C_{n,q} + F_{x_b,q}\Delta y_{cg} - F_{y_b,q}\Delta x_{cg} \tag{B.136}$$

$$M_{z_b,r} = \frac{1}{2}\rho V^2 S_w b_w C_{n,r} + F_{x_b,r}\Delta y_{cg} - F_{y_b,r}\Delta x_{cg} \tag{B.137}$$

J. Body-Fixed Force and Moment Derivatives with respect to Input

The body-fixed force and moment derivatives with respect to input will now be determined. Note, these equations also apply to either aircraft. The derivatives of the body-fixed x-force with respect to input are

$$F_{x_b,\delta_a} = \frac{1}{2}\rho V^2 S_w \left(C_{L,\delta_a} S_\alpha - C_{S,\delta_a} C_\alpha S_\beta - C_{D,\delta_a} C_\alpha C_\beta\right) \tag{B.138}$$

$$F_{x_b,\delta_e} = F_{x_b,\delta_e^B} = \frac{1}{2}\rho V^2 S_w \left(C_{L,\delta_e} S_\alpha - C_{S,\delta_e} C_\alpha S_\beta - C_{D,\delta_e} C_\alpha C_\beta\right) \tag{B.139}$$

$$F_{x_b,\delta_r} = \frac{1}{2}\rho V^2 S_w \left(C_{L,\delta_r} S_\alpha - C_{S,\delta_r} C_\alpha S_\beta - C_{D,\delta_r} C_\alpha C_\beta\right) \tag{B.140}$$

$$F_{x_b,\delta_B} = \frac{1}{2}\rho V^2 S_w \left(C_{L,\delta_B} S_\alpha - C_{S,\delta_B} C_\alpha S_\beta - C_{D,\delta_B} C_\alpha C_\beta\right) \tag{B.141}$$

$$F_{x_b,\tau} = T_{,\tau} \tag{B.142}$$

The derivatives of the body-fixed y-force with respect to input are

$$F_{y_b,\delta_a} = \frac{1}{2}\rho V^2 S_w \left(C_{S,\delta_a} C_\beta - C_{D,\delta_a} S_\beta\right) \tag{B.143}$$

$$F_{y_b,\delta_e} = F_{y_b,\delta_e^B} = \frac{1}{2}\rho V^2 S_w \left(C_{S,\delta_e} C_\beta - C_{D,\delta_e} S_\beta\right) \tag{B.144}$$

$$F_{y_b,\delta_r} = \frac{1}{2}\rho V^2 S_w \left(C_{S,\delta_r} C_\beta - C_{D,\delta_r} S_\beta\right) \tag{B.145}$$

$$F_{y_b,\delta_B} = \frac{1}{2}\rho V^2 S_w \left(C_{S,\delta_B} C_\beta - C_{D,\delta_B} S_\beta\right) \tag{B.146}$$

The derivatives of the body-fixed z-force with respect to input are

$$F_{z_b,\delta_a} = \frac{1}{2}\rho V^2 S_w \left(-C_{L,\delta_a} C_\alpha - C_{S,\delta_a} S_\alpha S_\beta - C_{D,\delta_a} S_\alpha C_\beta\right) \tag{B.147}$$

$$F_{z_b,\delta_e} = F_{z_b,\delta_e^B} = \frac{1}{2}\rho V^2 S_w \left(-C_{L,\delta_e} C_\alpha - C_{S,\delta_e} S_\alpha S_\beta - C_{D,\delta_e} S_\alpha C_\beta\right) \tag{B.148}$$

$$F_{z_b,\delta_r} = \frac{1}{2}\rho V^2 S_w \left(-C_{L,\delta_r} C_\alpha - C_{S,\delta_r} S_\alpha S_\beta - C_{D,\delta_r} S_\alpha C_\beta\right) \tag{B.149}$$

$$F_{z_b,\delta_B} = \frac{1}{2}\rho V^2 S_w \left(-C_{L,\delta_B} C_\alpha - C_{S,\delta_B} S_\alpha S_\beta - C_{D,\delta_B} S_\alpha C_\beta\right) \tag{B.150}$$

The derivatives of the body-fixed x-moment with respect to input are

$$M_{x_b,\delta_a} = \frac{1}{2}\rho V^2 S_w b_w C_{\ell,\delta_a} + F_{y_b,\delta_a}\Delta z_{cg} - F_{z_b,\delta_a}\Delta y_{cg} \tag{B.151}$$

$$M_{x_b,\delta_e} = M_{x_b,\delta_e^B} = \frac{1}{2}\rho V^2 S_w b_w C_{\ell,\delta_e} + F_{y_b,\delta_e}\Delta z_{cg} - F_{z_b,\delta_e}\Delta y_{cg} \tag{B.152}$$

$$M_{x_b,\delta_r} = \frac{1}{2}\rho V^2 S_w b_w C_{\ell,\delta_r} + F_{y_b,\delta_r}\Delta z_{cg} - F_{z_b,\delta_r}\Delta y_{cg} \tag{B.153}$$

$$M_{x_b,\delta_B} = \frac{1}{2}\rho V^2 S_w b_w C_{\ell,\delta_B} + F_{y_b,\delta_B}\Delta z_{cg} - F_{z_b,\delta_B}\Delta y_{cg} \tag{B.154}$$

The derivatives of the body-fixed y-moment with respect to input are

$$M_{y_b,\delta_a} = \frac{1}{2}\rho V^2 S_w \bar{c}_w C_{m,\delta_a} + F_{z_b,\delta_a}\Delta x_{cg} - F_{x_b,\delta_a}\Delta z_{cg} \tag{B.155}$$

$$M_{y_b,\delta_e} = M_{y_b,\delta_e^B} = \frac{1}{2}\rho V^2 S_w \bar{c}_w C_{m,\delta_e} + F_{z_b,\delta_e}\Delta x_{cg} - F_{x_b,\delta_e}\Delta z_{cg} \tag{B.156}$$

$$M_{y_b,\delta_r} = \frac{1}{2}\rho V^2 S_w \bar{c}_w C_{m,\delta_r} + F_{z_b,\delta_r}\Delta x_{cg} - F_{x_b,\delta_r}\Delta z_{cg} \tag{B.157}$$

$$M_{y_b,\delta_B} = \frac{1}{2}\rho V^2 S_w \bar{c}_w C_{m,\delta_B} + F_{z_b,\delta_B}\Delta x_{cg} - F_{x_b,\delta_B}\Delta z_{cg} \tag{B.158}$$

$$M_{y_b,\tau} = -F_{x_b,\tau}\Delta z_{cg} \tag{B.159}$$

The derivatives of the body-fixed z-moment with respect to input are

$$M_{z_b,\delta_a} = \frac{1}{2}\rho V^2 S_w b_w C_{n,\delta_a} + F_{x_b,\delta_a}\Delta y_{cg} - F_{y_b,\delta_a}\Delta x_{cg} \tag{B.160}$$

$$M_{z_b,\delta_e} = M_{z_b,\delta_e^B} = \frac{1}{2}\rho V^2 S_w b_w C_{n,\delta_e} + F_{x_b,\delta_e}\Delta y_{cg} - F_{y_b,\delta_e}\Delta x_{cg} \tag{B.161}$$

$$M_{z_b,\delta_r} = \frac{1}{2}\rho V^2 S_w b_w C_{n,\delta_r} + F_{x_b,\delta_r}\Delta y_{cg} - F_{y_b,\delta_r}\Delta x_{cg} \tag{B.162}$$

$$M_{z_b,\delta_B} = \frac{1}{2}\rho V^2 S_w b_w C_{n,\delta_B} + F_{x_b,\delta_B}\Delta y_{cg} - F_{y_b,\delta_B}\Delta x_{cg} \tag{B.163}$$

$$M_{z_b,\tau} = F_{x_b,\tau}\Delta y_{cg} \tag{B.164}$$

K. Linearized Formulation

The resulting linearized state dynamics matrix is

$$A_{\text{full}} = \begin{bmatrix} A_{V,V} & A_{V,\omega} & Z & A_{V,e} \\ A_{\omega,V} & A_{\omega,\omega} & Z & Z \\ A_{x,V} & Z & Z & A_{x,e} \\ Z & A_{e,\omega} & Z & A_{e,e} \end{bmatrix} \tag{B.165}$$

where the body-fixed acceleration matrix components are

$$A_{V,V} = \begin{bmatrix} \frac{g}{W}F_{x_b,V_{x_b}} & \frac{g}{W}F_{x_b,V_{y_b}} + r & \frac{g}{W}F_{x_b,V_{z_b}} - q \\ \frac{g}{W}F_{y_b,V_{x_b}} - r & \frac{g}{W}F_{y_b,V_{y_b}} & \frac{g}{W}F_{y_b,V_{z_b}} + p \\ \frac{g}{W}F_{z_b,V_{x_b}} + q & \frac{g}{W}F_{z_b,V_{y_b}} - p & \frac{g}{W}F_{z_b,V_{z_b}} \end{bmatrix} \tag{B.166}$$

$$A_{V,\omega} = \begin{bmatrix} \frac{g}{W}F_{x_b,p} & \frac{g}{W}F_{x_b,q} - V_{z_b} & \frac{g}{W}F_{x_b,r} + V_{y_b} \\ \frac{g}{W}F_{y_b,p} + V_{z_b} & \frac{g}{W}F_{y_b,q} & \frac{g}{W}F_{y_b,r} - V_{x_b} \\ \frac{g}{W}F_{z_b,p} - V_{y_b} & \frac{g}{W}F_{z_b,q} + V_{x_b} & \frac{g}{W}F_{z_b,r} \end{bmatrix} \tag{B.167}$$

$$A_{V,e} = g \begin{bmatrix} 0 & -C_\theta & 0 \\ C_\phi C_\theta & -S_\phi S_\theta & 0 \\ -S_\phi C_\theta & -C_\phi S_\theta & 0 \end{bmatrix} \tag{B.168}$$

the body-fixed angular-acceleration matrix components are

$$A_{\omega,V} = [\mathbf{I}]^{-1} \begin{bmatrix} M_{x_b,V_{x_b}} & M_{x_b,V_{y_b}} & M_{x_b,V_{z_b}} \\ M_{y_b,V_{x_b}} & M_{y_b,V_{y_b}} & M_{y_b,V_{z_b}} \\ M_{z_b,V_{x_b}} & M_{z_b,V_{y_b}} & M_{z_b,V_{z_b}} \end{bmatrix} \tag{B.169}$$

$$\begin{aligned} A_{\omega,\omega} = [\mathbf{I}]^{-1} \Bigg[& \begin{bmatrix} M_{x_b,p} & M_{x_b,q} & M_{x_b,r} \\ M_{y_b,p} & M_{y_b,q} & M_{y_b,r} \\ M_{z_b,p} & M_{z_b,q} & M_{z_b,r} \end{bmatrix} + \begin{bmatrix} 0 & -h_{z_b} & h_{y_b} \\ h_{z_b} & 0 & -h_{x_b} \\ -h_{y_b} & h_{x_b} & 0 \end{bmatrix} \\ & + \begin{bmatrix} I_{xz_b}q - I_{xy_b}r & (I_{yy_b} - I_{zz_b})r + 2I_{yz_b}q + I_{xz_b}p & (I_{yy_b} - I_{zz_b})q - 2I_{yz_b}r - I_{xy_b}p \\ (I_{zz_b} - I_{xx_b})r - 2I_{xz_b}p - I_{yz_b}q & I_{xy_b}r - I_{yz_b}p & (I_{zz_b} - I_{xx_b})p + 2I_{xz_b}r + I_{xy_b}q \\ (I_{xx_b} - I_{yy_b})q + 2I_{xy_b}p + I_{yz_b}r & (I_{xx_b} - I_{yy_b})p - 2I_{xy_b}q - I_{xz_b}r & I_{yz_b}p - I_{xz_b}q \end{bmatrix} \Bigg] \end{aligned} \tag{B.170}$$

In order to simplify the numerical computation, the analytic inverse of the inertia tensor will be defined, as

$$[\mathbf{I}]^{-1} = \begin{bmatrix} I_{xx_b} & -I_{xy_b} & -I_{xz_b} \\ -I_{xy_b} & I_{yy_b} & -I_{yz_b} \\ -I_{xz_b} & -I_{yz_b} & I_{zz_b} \end{bmatrix}^{-1} = \frac{1}{|\mathbf{I}|} \begin{bmatrix} I_{yy_b}I_{zz_b} - I_{yz_b}^2 & I_{xy_b}I_{zz_b} + I_{xz_b}I_{yz_b} & I_{xy_b}I_{yz_b} + I_{xz_b}I_{yy_b} \\ I_{xy_b}I_{zz_b} + I_{xz_b}I_{yz_b} & I_{xx_b}I_{zz_b} - I_{xz_b}^2 & I_{xx_b}I_{yz_b} + I_{xy_b}I_{xz_b} \\ I_{xy_b}I_{yz_b} + I_{xz_b}I_{yy_b} & I_{xx_b}I_{yz_b} + I_{xy_b}I_{xz_b} & I_{xx_b}I_{yy_b} - I_{xy_b}^2 \end{bmatrix} \tag{B.171}$$

where the determinant of the inertia tensor is

$$|\mathbf{I}| = I_{xx_b}(I_{yy_b}I_{zz_b} - I_{yz_b}^2) - 2I_{xy_b}I_{xz_b}I_{yz_b} - (I_{xy_b}^2 I_{zz_b} + I_{xz_b}^2 I_{yy_b}) \tag{B.172}$$

the Earth-fixed velocity matrix components are

$$A_{x,V} = \begin{bmatrix} C_\theta C_\psi & S_\phi S_\theta C_\psi - C_\phi S_\psi & C_\phi S_\theta C_\psi + S_\phi S_\psi \\ C_\theta S_\psi & S_\phi S_\theta S_\psi + C_\phi C_\psi & C_\phi S_\theta S_\psi - S_\phi C_\psi \\ -S_\theta & S_\phi C_\theta & C_\phi C_\theta \end{bmatrix} \tag{B.173}$$

$$A_{x,e} = \begin{bmatrix} V_{y_f} S_\theta C_\psi + V_{z_f} S_\psi & V_{z_f} C_\theta C_\psi - S_\theta C_\psi V_{x_b} & -V_{y_f} C_\psi - \left(V_{z_f} S_\theta + C_\theta V_{x_b} \right) S_\psi \\ V_{y_f} S_\theta S_\psi - V_{z_f} C_\psi & V_{z_f} C_\theta S_\psi - S_\theta S_\psi V_{x_b} & -V_{y_f} S_\psi + \left(V_{z_f} S_\theta + C_\theta V_{x_b} \right) C_\psi \\ V_{y_f} C_\theta & -C_\theta V_{x_b} - V_{z_f} S_\theta & 0 \end{bmatrix} \tag{B.174}$$

$$V_{y_f} = C_\phi V_{y_b} - S_\phi V_{z_b} \tag{B.175}$$

$$V_{z_f} = S_\phi V_{y_b} + C_\phi V_{z_b} \tag{B.176}$$

and the Earth-fixed orientation-rates matrix components are

$$A_{e,\omega} = \begin{bmatrix} 1 & S_\phi S_\theta / C_\theta & C_\phi S_\theta / C_\theta \\ 0 & C_\phi & -S_\phi \\ 0 & S_\phi / C_\theta & C_\phi / C_\theta \end{bmatrix} \tag{B.177}$$

$$A_{e,e} = \begin{bmatrix} C_\phi S_\theta / C_\theta q - S_\phi S_\theta / C_\theta r & \left(S_\phi q + C_\phi r \right) / C_\theta^2 & 0 \\ -S_\phi q - C_\phi r & 0 & 0 \\ \left(C_\phi q - S_\phi r \right) / C_\theta & \left(S_\phi q + C_\phi r \right) S_\theta / C_\theta^2 & 0 \end{bmatrix} \tag{B.178}$$

with the zero matrix

$$Z = \begin{bmatrix} 0 & 0 & 0 \\ 0 & 0 & 0 \\ 0 & 0 & 0 \end{bmatrix} \tag{B.179}$$

Where some states are neglected (see Eq. (51)) from the feedback control design, the linearized state dynamics matrix is

$$A = C A_{\text{full}} C^T = \begin{bmatrix} A_{V,V} & A_{V,\omega} & Z C_x^T & A_{V,e} C_e^T \\ A_{\omega,V} & A_{\omega,\omega} & Z C_x^T & Z C_e^T \\ C_x A_{x,V} & C_x Z & C_x Z C_x^T & C_x A_{x,e} C_e^T \\ C_e Z & C_e A_{e,\omega} & C_e Z C_x^T & C_e A_{e,e} C_e^T \end{bmatrix} \tag{B.180}$$

where

$$C_e = \begin{bmatrix} 1 & 0 & 0 \\ 0 & 1 & 0 \end{bmatrix} \tag{B.181}$$

$$C_x = \begin{bmatrix} 0 & 0 & 1 \end{bmatrix} \tag{B.182}$$

The resulting linearized input dynamics matrix is

$$B_{\text{full}} = \begin{bmatrix} B_{V,u} \\ B_{\omega,u} \\ Z_q \\ Z_q \end{bmatrix} \tag{B.183}$$

where, for the baseline aircraft, the body-fixed acceleration and angular-acceleration matrix components are

$$B_{V,u} = \frac{g}{W} \begin{bmatrix} F_{x_b,\delta_a} & F_{x_b,\delta_e} & F_{x_b,\delta_r} & F_{x_b,\tau} \\ F_{y_b,\delta_a} & F_{y_b,\delta_e} & F_{y_b,\delta_r} & 0 \\ F_{z_b,\delta_a} & F_{z_b,\delta_e} & F_{z_b,\delta_r} & 0 \end{bmatrix} \tag{B.184}$$

$$B_{\omega,u} = [\mathbf{I}]^{-1} \begin{bmatrix} M_{x_b,\delta_a} & M_{x_b,\delta_e} & M_{x_b,\delta_r} & 0 \\ M_{y_b,\delta_a} & M_{y_b,\delta_e} & M_{y_b,\delta_r} & M_{y_b,\tau} \\ M_{z_b,\delta_a} & M_{z_b,\delta_e} & M_{z_b,\delta_r} & M_{z_b,\tau} \end{bmatrix} \tag{B.185}$$

and for the BIRE, the body-fixed acceleration and angular-acceleration matrix components are

$$B_{V,u} = \frac{g}{W}\begin{bmatrix} F_{x_b,\delta_a} & F_{x_b,\delta_e^B} & F_{x_b,\delta_B} & F_{x_b,\tau} \\ F_{y_b,\delta_a} & F_{y_b,\delta_e^B} & F_{y_b,\delta_B} & 0 \\ F_{z_b,\delta_a} & F_{z_b,\delta_e^B} & F_{z_b,\delta_B} & 0 \end{bmatrix} \tag{B.186}$$

$$B_{\omega,u} = [\hat{\mathbf{I}}]^{-1}\begin{bmatrix} M_{x_b,\delta_a} & M_{x_b,\delta_e^B} & \dot{p}_{,\delta_B} & 0 \\ M_{y_b,\delta_a} & M_{y_b,\delta_e^B} & \dot{q}_{,\delta_B} & M_{y_b,\tau} \\ M_{z_b,\delta_a} & M_{z_b,\delta_e^B} & \dot{r}_{,\delta_B} & M_{z_b,\tau} \end{bmatrix} + [\breve{\mathbf{I}}]^{-1}\begin{bmatrix} 0 & 0 & \dot{p} & 0 \\ 0 & 0 & \dot{q} & 0 \\ 0 & 0 & \dot{r} & 0 \end{bmatrix} \tag{B.187}$$

in which

$$\begin{bmatrix} \dot{p}_{,\delta_B} \\ \dot{q}_{,\delta_B} \\ \dot{r}_{,\delta_B} \end{bmatrix} = \left[\begin{bmatrix} M_{x_b,\delta_B} \\ M_{y_b,\delta_B} \\ M_{z_b,\delta_B} \end{bmatrix} + \begin{bmatrix} (\breve{I}_{yy_b} - \breve{I}_{zz_b})qr + \breve{I}_{yz_b}(q^2 - r^2) + \breve{I}_{xz_b}pq - \breve{I}_{xy_b}pr \\ (\breve{I}_{zz_b} - \breve{I}_{xx_b})pr + \breve{I}_{xz_b}(r^2 - p^2) + \breve{I}_{xy_b}qr - \breve{I}_{yz_b}pq \\ (\breve{I}_{xx_b} - \breve{I}_{yy_b})pq + \breve{I}_{xy_b}(p^2 - q^2) + \breve{I}_{yz_b}pr - \breve{I}_{xz_b}qr \end{bmatrix}\right] \tag{B.188}$$

and (from Eq. (40))

$$\begin{bmatrix} \dot{p} \\ \dot{q} \\ \dot{r} \end{bmatrix} = \left[\begin{bmatrix} M_{x_b} \\ M_{y_b} \\ M_{z_b} \end{bmatrix} + \begin{bmatrix} 0 & -h_{z_b} & h_{y_b} \\ h_{z_b} & 0 & -h_{x_b} \\ -h_{y_b} & h_{x_b} & 0 \end{bmatrix}\begin{bmatrix} p \\ q \\ r \end{bmatrix} + \begin{bmatrix} (\hat{I}_{yy_b} - \hat{I}_{zz_b})qr + \hat{I}_{yz_b}(q^2 - r^2) + \hat{I}_{xz_b}pq - \hat{I}_{xy_b}pr \\ (\hat{I}_{zz_b} - \hat{I}_{xx_b})pr + \hat{I}_{xz_b}(r^2 - p^2) + \hat{I}_{xy_b}qr - \hat{I}_{yz_b}pq \\ (\hat{I}_{xx_b} - \hat{I}_{yy_b})pq + \hat{I}_{xy_b}(p^2 - q^2) + \hat{I}_{yz_b}pr - \hat{I}_{xz_b}qr \end{bmatrix}\right] \tag{B.189}$$

where the BIRE-angle derivative of the inverted inertia tensor is

$$[\breve{\mathbf{I}}]^{-1} = \frac{1}{|\hat{\mathbf{I}}|}\,\mathrm{adj}\left(|\breve{\mathbf{I}}|\right) - [\hat{\mathbf{I}}]^{-1}\frac{|\breve{\mathbf{I}}|}{|\hat{\mathbf{I}}|} \tag{B.190}$$

$$\mathrm{adj}\left(|\breve{\mathbf{I}}|\right) = \begin{bmatrix} \breve{I}_{yy_b}\hat{I}_{zz_b} + \hat{I}_{yy_b}\breve{I}_{zz_b} - 2\hat{I}_{yz_b}\breve{I}_{yz_b} & I_a & I_b \\ I_a & \breve{I}_{xx_b}\hat{I}_{zz_b} + \hat{I}_{xx_b}\breve{I}_{zz_b} - 2\hat{I}_{xz_b}\breve{I}_{xz_b} & I_c \\ I_b & I_c & \breve{I}_{xx_b}\hat{I}_{yy_b} + \hat{I}_{xx_b}\breve{I}_{yy_b} - 2\hat{I}_{xy_b}\breve{I}_{xy_b} \end{bmatrix} \tag{B.191}$$

$$I_a = \breve{I}_{xy_b}\hat{I}_{zz_b} + \hat{I}_{xy_b}\breve{I}_{zz_b} + \breve{I}_{xz_b}\hat{I}_{yz_b} + \hat{I}_{xz_b}\breve{I}_{yz_b} \tag{B.192}$$

$$I_b = \breve{I}_{xy_b}\hat{I}_{yz_b} + \hat{I}_{xy_b}\breve{I}_{yz_b} + \breve{I}_{xz_b}\hat{I}_{yy_b} + \hat{I}_{xz_b}\breve{I}_{yy_b} \tag{B.193}$$

$$I_c = \breve{I}_{xx_b}\hat{I}_{yz_b} + \hat{I}_{xx_b}\breve{I}_{yz_b} + \breve{I}_{xy_b}\hat{I}_{xz_b} + \hat{I}_{xy_b}\breve{I}_{xz_b} \tag{B.194}$$

$$\begin{aligned} |\breve{\mathbf{I}}| = {} & \breve{I}_{xx_b}(\hat{I}_{yy_b}\hat{I}_{zz_b} - \hat{I}_{yz_b}^2) + \hat{I}_{xx_b}(\breve{I}_{yy_b}\hat{I}_{zz_b} + \hat{I}_{yy_b}\breve{I}_{zz_b} - 2\hat{I}_{yz_b}\breve{I}_{yz_b}) - 2\breve{I}_{xy_b}\hat{I}_{xz_b}\hat{I}_{yz_b} - 2\hat{I}_{xy_b}\breve{I}_{xz_b}\hat{I}_{yz_b} \\ & - 2\hat{I}_{xy_b}\hat{I}_{xz_b}\breve{I}_{yz_b} - (2\hat{I}_{xy_b}\breve{I}_{xy_b}\hat{I}_{zz_b} + \hat{I}_{xy_b}^2\breve{I}_{zz_b} + 2\hat{I}_{xz_b}\breve{I}_{xz_b}\hat{I}_{yy_b} + \hat{I}_{xz_b}^2\breve{I}_{yy_b}) \end{aligned} \tag{B.195}$$

or for the specific case of the BIRE aircraft ($\hat{I}_{xy_b} = \breve{I}_{xy_b} = \breve{I}_{xx_b} = \breve{I}_{xz_b} = 0$)

$$[\breve{\mathbf{I}}]^{-1} = \frac{1}{|\mathbf{I}|}\begin{bmatrix} \breve{I}_{yy_b}\hat{I}_{zz_b} + \hat{I}_{yy_b}\breve{I}_{zz_b} - 2\hat{I}_{yz_b}\breve{I}_{yz_b} & \hat{I}_{xz_b}\breve{I}_{yz_b} & \hat{I}_{xz_b}\breve{I}_{yy_b} \\ \hat{I}_{xz_b}\breve{I}_{yz_b} & \hat{I}_{xx_b}\breve{I}_{zz_b} & \hat{I}_{xx_b}\breve{I}_{yz_b} \\ \hat{I}_{xz_b}\breve{I}_{yy_b} & \hat{I}_{xx_b}\breve{I}_{yz_b} & \hat{I}_{xx_b}\breve{I}_{yy_b} \end{bmatrix} - [\mathbf{I}]^{-1}\frac{|\breve{\mathbf{I}}|}{|\mathbf{I}|} \tag{B.196}$$

$$|\breve{\mathbf{I}}| = \hat{I}_{xx_b}(\breve{I}_{yy_b}\hat{I}_{zz_b} + \hat{I}_{yy_b}\breve{I}_{zz_b} - 2\hat{I}_{yz_b}\breve{I}_{yz_b}) - \hat{I}_{xz_b}^2\breve{I}_{yy_b} \tag{B.197}$$

and the zero matrix

$$Z_q = \begin{bmatrix} 0 & 0 & 0 & 0 \\ 0 & 0 & 0 & 0 \\ 0 & 0 & 0 & 0 \end{bmatrix} \tag{B.198}$$

Where some states are neglected (see Eq. (51)) from the feedback control design, the linearized input dynamics matrix is

$$B = CB_{\text{full}} = \begin{bmatrix} B_{V,u} \\ B_{\omega,u} \\ C_x Z_q \\ C_e Z_q \end{bmatrix} = \begin{bmatrix} B_{V,u} \\ B_{\omega,u} \\ Z_q \end{bmatrix} \tag{B.199}$$

The inertia tensor components I_{xx_b}, I_{yy_b}, I_{zz_b}, I_{xy_b}, and I_{xz_b} follow the format given in Eq. (17). I_{yz_b} however, does not and follows the form

$$\hat{I}_{yz_b} = A\,|\sin(\omega\delta_B + \phi)| + z \tag{B.200}$$

thus having the BIRE-angle derivative

$$\check{I}_{yz_b} = A\omega\frac{\sin(\omega\delta_B + \phi)\cos(\omega\delta_B + \phi)}{|\sin(\omega\delta_B + \phi)|} \tag{B.201}$$

As noted by Bolander, this derivative is undefined when the BIRE angle $\delta_B = 0°, \pm 180°$, and as stated by Bolander, this derivative will be set to zero at these conditions [6]. The limit of this derivative as δ_B approaches zero is -1 approached from negative infinity and +1 approached from positive infinity. Taking both directions into account, and when viewing the form of $\hat{I}_{yz_b}$ graphically, it can be readily seen that a value of zero is most appropriate for the cases of $\delta_B = 0°, \pm 180°$.

Acknowledgments

This work was funded by the Air Force Office of Scientific Research (AFOSR) Lab Task 23RQCOR006 with Dr. Les Lee as the program manager. This paper has been cleared for public release, Case Number: AFRL-2023-5564.

References

[1] Bolander, C. R., Hunsaker, D. F., Myszka, D., and Joo, J. J., "Attainable Moment Set and Actuation Time of a Bio-Inspired Rotating Empennage," *AIAA SciTech 2022 Forum*, American Institute of Aeronautics and Astronautics, San Diego, CA, 2022, p. 1670. .

[2] Ives, C., Myszka, D. H., Joo, J., Bolander, C. R., and Hunsaker, D. F., "Using a Topology Optimization Results Interpreter on the Frame of an Aircraft with a Bio-Inspired Rotating Empennage," *AIAA Aviation 2022 Forum*, 2022, p. 3373. .

[3] Kohler, A. J., Bolander, C. R., Hunsaker, D. F., and Joo, J. J., "Linearized Rigid-Body Static and Dynamic Stability of an Aircraft with a Bio-Inspired Rotating Empennage," *AIAA SciTech 2023 Forum*, 2023, p. 0621. .

[4] Abraham, T. A., Hunsaker, D. F., and Joo, J. J., "A Generalized Linear Dynamic Modes Analysis Applied To Non-Symmetric Aircraft," , 2024. AIAA SciTech 2024 Forum : submitted.

[5] Bolander, C. R., Kohler, A. J., Hunsaker, D. F., Myszka, D., and Joo, J. J., "Static Trim of a Bio-Inspired Rotating Empennage for a Fighter Aircraft," *AIAA SciTech 2023 Forum*, 2023, p. 0624. .

[6] Bolander, C. R., "Aerodynamic Implications of a Bio-Inspired Rotating Empennage Design for Control of a Fighter Aircraft," Ph.D. thesis, Utah State University, 2023. .

[7] Stevens, B. L., and Lewis, F. L., *Aircraft Control and Simulation*, 2nd ed., John Wiley & Sons, Inc., 2003.

[8] Lewis, F. L., Vrabie, D. L., and Syrmos, V. L., *Optimal Control*, John Wiley & Sons, 2012.

[9] Blakelock, J. H., *Automatic Control of Aircraft and Missiles*, 2nd ed., John Wiley & Sons, 1991.

[10] Skogestad, S., and Postlethwaite, I., *Multivariable Feedback Control : Analysis and Design*, 2nd ed., John Wiley & Sons, Inc., 2005.

[11] Bryson, A. E., *Applied Linear Optimal Control: Examples and Algorithms*, Cambridge University Press, 2002.

[12] Khalil, H. K., *Nonlinear Systems*, 3rd ed., Prentice Hall, 2002.

[13] Rugh, W. J., *Nonlinear System Theory*, Johns Hopkins University Press Baltimore, 1981.

[14] Lavretsky, E., and Wise, K. A., *Robust and Adaptive Control : with Aerospace Applications*, Springer, 2013.

[15] Stengel, R. F., *Flight Dynamics*, 2nd ed., Princeton University Press, 2022.

[16] Stevens, B. L., and Lewis, F. L., "Modern Design Techniques : Linear Quadratic Design with Full State Feedback," *Aircraft Control and Simulation*, John Wiley & Sons, Inc., 2003, 2nd ed., pp. 478–484.

[17] Skogestad, S., and Postlethwaite, I., "Controller Design : LQG control," *Multivariable Feedback Control : Analysis and Design*, John Wiley & Sons, Inc., 2005, 2nd ed., pp. 344–352.

[18] Nepomuceno, L., Moura, É. A., Morales, M. A., Silva, R. G., and Góes, L. C., "An LQR-LMI Longitudinal Stability Augmentation System for a Subscale Fighter Aircraft with Variable Center of Gravity Position," *AIAA Aviation 2022 Forum*, 2022, p. 4059. .

[19] Rademakers, N. G. M., "Control of a Tailless Fighter Using Gain-Scheduling," Tech. Rep. DCT.2004.19, Eindhoven University of Technology, Netherlands, 2004.

[20] Chrif, L., and Kadda, Z. M., "Aircraft Control System using LQG and LQR Controller with Optimal Estimation-Kalman Filter Design," *Procedia Engineering*, Vol. 80, 2014, pp. 245–257. .

[21] Usta, M. A., Akyazi, Ö., and Akpinar, A. S., "Aircraft Roll Control System using LQR and Fuzzy Logic Controller," *2011 International Symposium on Innovations in Intelligent Systems and Applications*, IEEE, 2011, pp. 223–227. .

[22] Ahmad, H., Young, T., Toal, D., and Omerdic, E., "Control Allocation with Actuator Dynamics for Aircraft Flight Controls," *7th AIAA ATIO Conf, 2nd CEIAT Int'l Conf on Innov and Integr in Aero Sciences, 17th LTA Systems Tech Conf; followed by 2nd TEOS Forum*, 2007, p. 7828. .

[23] Garrard, W. L., Enns, D. F., and Antony Snell, S., "Nonlinear Feedback Control of Highly Manoeuverable Aircraft," *International Journal of Control*, Vol. 56, No. 4, 1992, pp. 799–812. .

[24] Ashraf, A., Mei, W., Gaoyuan, L., Anjum, Z., and Kamal, M. M., "Design Linear Feedback and LQR Controller for Lateral Flight Dynamics of F-16 Aircraft," *2018 International Conference on Control, Automation and Information Sciences (ICCAIS)*, IEEE, 2018, pp. 367–371. .

[25] Ashraf, A., Mei, W., Gaoyuan, L., Kamal, M. M., and Mutahir, A., "Linear Feedback and LQR Controller Design for Aircraft Pitch Control," *2018 IEEE 4th International Conference on Control Science and Systems Engineering (ICCSSE)*, 2018, pp. 276–278. .

[26] Bhattacharya, R., "Robust LQR Design for Systems with Probabilistic Uncertainty," *International Journal of Robust and Nonlinear Control*, Vol. 29, No. 10, 2019, pp. 3217–3237. .

[27] Mortazavi, M. R., and Naghash, A., "Pitch and Flight Path Controller Design for F-16 Aircraft using Combination of LQR and EA Techniques," *Proceedings of the Institution of Mechanical Engineers, Part G: Journal of Aerospace Engineering*, Vol. 232, No. 10, 2018, pp. 1831–1843. .

[28] Fisher, J., and Bhattacharya, R., "On Stochastic LQR Design and Polynomial Chaos," *2008 American Control Conference*, 2008, pp. 95–100. .

[29] Tadiparthi, V., and Bhattacharya, R., "Robust LQR for Uncertain Discrete-Time Systems using Polynomial Chaos," *2020 American Control Conference (ACC)*, 2020, pp. 4472–4477. .

[30] Halder, A., Lee, K., and Bhattacharya, R., "Probabilistic Robustness Analysis of F-16 Controller Performance: An Optimal Transport Approach," *2013 American Control Conference*, 2013, pp. 5562–5567. .

[31] Ahmed, W., Li, Z., Maqsood, H., and Anwar, B., "System Modeling and Controller Design for Lateral and Longitudinal Motion of F-16," *Automation Control and Intelligent Systems*, Vol. 4, No. 1, 2019, pp. 39–45. .

[32] Fekri, M., and Mobed, M., "Angle of Attack Estimation and Aircraft Controller Design using LQR Methods," *Canadian Conference on Electrical and Computer Engineering, 2005.*, 2005, pp. 2253–2256. .

[33] Wagner, D. R., Henrion, D., and Hromčík, M., "Measures and LMIs for Validation of an Aircraft with MRAC and Uncertain Actuator Dynamics," *AIAA Scitech 2021 Forum*, 2021, p. 0531. .

[34] Chandler, P., Mears, M., and Pachter, M., "A Hybrid LQR/LP Approach for Addressing Actuator Saturation in Feedback Control," *Proceedings of 1994 33rd IEEE Conference on Decision and Control*, 1994, pp. 3860–3867. .

[35] Zollitsch, A. W., Holzapfel, F., and Annaswamy, A. M., "Application of Adaptive Control with Closed-Loop Reference Models to a Model Aircraft with Actuator Dynamics and Input Uncertainty," *2015 American Control Conference (ACC)*, 2015, pp. 3848–3853. .

[36] Vo, H., and Seshagiri, S., "Robust Control of F-16 Lateral Dynamics," *2008 34th annual conference of IEEE industrial electronics*, IEEE, 2008, pp. 343–348. .

[37] Royer, C., and Mavris, D., "Optimal Flight Control with Nonlinear Actuator Compensation through Model Reference Adaptive Control," *AIAA Guidance, Navigation, and Control Conference*, 2012, p. 4770. .

[38] Adams, R., Buffington, J., and Banda, S., "Active Vortex Flow Control for VISTA F-16 Envelope Expansion," *Guidance, Navigation, and Control Conference*, 1994, p. 3681. .

[39] Nguyen, L., Ogburn, M., Gilbert, W., Kibler, K., Brown, P., and Deal, P., "Simulation Study of Stall/Post-Stall Characteristics of a Fighter Airplane With Relaxed Static Stability," Tech. Rep. NASA-TP-1538, NASA Langley Research Center, Hampton, 1979. .

[40] Phillips, W. F., "Fluid Statics and the Atmosphere," *Mechanics of Flight*, John Wiley & Sons, Inc., Hoboken, 2010, 2nd ed., pp. 10–14.

[41] Stengel, R. F., *Flight Dynamics*, Princeton University Press, 2004.

[42] Beard, R. W., and McLain, T. W., *Small Unmanned Aircraft: Theory and Practice*, Princeton university press, 2012.

[43] Anderson, J. D., "Aerodynamics of the Airplane : The Drag Polar : Lift and Drag Buildup," *Aircraft Performance & Design*, McGraw-Hill, 1999, pp. 78–126.

[44] Department of Defense, "Flying Qualities of Piloted Airplanes," Tech. Rep. MIL-F-8785C, Department of Defense, 1980.

[45] Beal, T. R., "Digital Simulation of Atmospheric Turbulence for Dryden and von Karman Models," *Journal of Guidance, Control, and Dynamics*, Vol. 16, 1993, pp. 132–138.

[46] Chapra, S. C., and Cananle, R. P., *Numerical Methods for Engineers*, 7th ed., McGraw-Hill, New York, 2015.

[47] Roetman, E., Northcraft, S., and Dawdy, J., "Innovative Control Effectors (ICE)," Tech. Rep. 96-3074, Boeing Defense and Space Group, 1996.

[48] Dorsett, K. M., and Mehl, D. R., "Innovative Control Effectors (ICE)," Tech. Rep. 96-3043, Lockheed Martin Tactical Aircraft Systems, 1996.

[49] Phillips, W. F., "Linearized Longitudinal Dynamics : Longitudinal Motion: The Linearized Coupled Equations," *Mechanics of Flight*, John Wiley & Sons, Inc., 2010, Chap. 8, 2nd ed., pp. 836–846.

[50] Phillips, W. F., "Linearized Lateral Dynamics : Lateral Motion: The Linearized Coupled Equations," *Mechanics of Flight*, John Wiley & Sons, Inc., 2010, Chap. 9, 2nd ed., pp. 885–895.

[51] of Defense, U. S. D., "Military Specification - Flying Qualities of Piloted Airplanes," Tech. Rep. MIL-F-8785C, United States Department of Defense, 1980.

[52] Hodgkinson, J., *Aircraft Handling Qualities*, AIAA Education Series, 1999.

[53] Phillips, W. F., "Aircraft Handling Qualities and Control Response : Dynamic Handling Quality Prediction," *Mechanics of Flight*, John Wiley & Sons, Inc., 2010, Chap. 10, 2nd ed., pp. 958–968.

[54] Phillips, W. F., "Aircraft Flight Simulation," *Mechanics of Flight*, John Wiley & Sons, Inc., 2010, Chap. 11, 2nd ed., pp. 989–1068.